Liquefaction Resistance Evaluation of Soils using Artificial Neural Network for Dhaka City, Bangladesh

Abul Kashem Faruki Fahim
University of Dhaka Faculty of Earth and Environmental Sciences
Md. Zillur Rahman
University of Dhaka Faculty of Earth and Environmental Sciences
Md. Shakhawat Hossain
University of Dhaka Faculty of Earth and Environmental Sciences
A S M Maksud Kamal (maksudkamal@du.ac.bd)
University of Dhaka Faculty of Earth and Environmental Sciences https://orcid.org/0000-0002-3896-2032

Research Article

Keywords: Earthquake, Liquefaction, Liquefaction potential index (LPI), Simplified procedure, Artificial neural network (ANN)

Posted Date: May 18th, 2021

DOI: https://doi.org/10.21203/rs.3.rs-468975/v1

Liquefaction resistance evaluation of soils using artificial neural network for Dhaka City, Bangladesh

Abul Kashem Faruki Fahim, Md. Zillur Rahman, Md. Shakhawat Hossain, and A. S. M. Maksud Kamal*

Department of Disaster Science and Management, University of Dhaka, Dhaka 1000, Bangladesh

*__Corresponding Author__: Dr. A. S. M. Maksud Kamal, Professor, Department of Disaster Science and Management, University of Dhaka, Dhaka 1000, Bangladesh

e-mail: maksudkamal@du.ac.bd, cell: +880-1759760944

Abstract

Soil liquefaction resistance evaluation is an important site investigation for seismically active areas. To minimize the loss of life and property, liquefaction hazard analysis is a prerequisite for seismic risk management and development of an area. Liquefaction potential index (LPI) is widely used to determine the severity of liquefaction quantitatively and spatially. LPI is estimated from the factor of safety (FS) of liquefaction that is the ratio of cyclic resistance ratio (CRR) to cyclic stress ratio (CSR) calculated applying simplified procedure. Artificial neural network (ANN) algorithm has been used in the present study to predict CRR directly from the normalized standard penetration test blow count (SPT-N) and near-surface shear wave velocity (V_s) data of Dhaka City. It is observed that ANN model have generated accurate CRR data. Three liquefaction hazard zones are identified in Dhaka City on the basis of the cumulative frequency (CF) distribution of the LPI of each geological unit. The liquefaction hazard maps have been prepared for the city using the liquefaction potential index (LPI) and its cumulative frequency (CF) distribution of each liquefaction hazard zone. The CF distribution of the SPT-N based LPI indicates that 15%, 53%, and 69% of areas, whereas the CF distribution of the V_s based LPI indicates that 11%, 48%, and 62% of areas of Zone 1, 2, and 3, respectively, show surface manifestation of liquefaction for a scenario earthquake of moment magnitude, M_w 7.5 with a peak horizontal ground acceleration (PGA) of 0.15 g.

Keywords: Earthquake, Liquefaction, Liquefaction potential index (LPI), Simplified procedure, Artificial neural network (ANN)

1. Introduction

Liquefaction occurs when granular, loosely compacted or cohesionless, saturated or partially saturated sediments lose their shear strength and transform from solid to liquid state at or near the ground surface resulting from cyclic loading or other abrupt alteration of stress conditions (Castro 1969; Castro and Poulos 1977; Castro et al. 1982). The loss of strength takes place in cohesionless soil due to reduction in effective stress resulting from increased pore water pressure caused by rapid, usually cyclic loading exerted by strong ground shaking (Marcuson 1978).

During an earthquake, liquefaction can be devastating incurring widespread damage, which was revealed by Niigata Earthquake in 1964, Alaska Earthquake in 1964, Loma Prieta Earthquake in 1989, Chi-Chi Earthquake in 1999, and Sulawesi Earthquake in 2018 (Seed and Idriss 1967; Ku et al. 2004; Lee et al. 2007; Chao et al. 2010; Sassa and Takagawa 2019; Hossain et al. 2020). Therefore, in a seismic hazard-prone area, liquefaction resistance evaluation is an integral part of site characterization.

Both in situ tests (e.g., SPT, V_s, Cone Penetration Test (CPT) data) and soil laboratory tests (e.g., cyclic triaxial test) can be used to evaluate soil liquefaction resistance during seismic loading. Good-quality undisturbed soil samples are essential to assess the soil liquefaction resistance by the laboratory tests. However, collecting such samples from degraded loosely compacted silty or sandy soils are sometimes difficult and expensive. Due to these drawbacks of the laboratory tests, geotechnical engineers widely use in situ tests as it is simple and economical (Seed and Idriss 1971, 1982; Seed et al. 1983, 1984, 1985; Seed and de Alba 1986). Over the last five decades, the Simplified Procedure, developed initially by Seed and Idriss (1971), has been used in liquefaction resistance evaluation of soils. Since its inception in 1971, many researchers have updated, modified, revised, and validated this method (e.g., Juang et al. 2003, 2000; Olsen 1997, 1988; Olsen and Koester 1995; Robertson and Wride 1998; Stark and Olson 1995). To assess liquefaction resistance by this procedure, the corrected SPT-N is widely used as input (Seed and Idriss 1971, 1982; Seed et al. 1983, 1984, 1985; Kayen et al. 1992; Juang et al. 2000; Youd et al. 2001; Idriss and Boulanger 2004).

Using field V_s measurement, a method of liquefaction resistance estimation was introduced by Andrus et al. (2000) and Andrus and Stokoe (1997). The use of the V_s data has more advantages than the SPT-N and CPT data as the V_s data can easily be collected from stiff and gravelly soils. The soil profile can be easily obtained and the

analytical procedures that analyze the small-scale shear modulus for evaluating soil-structure interaction and dynamic soil response are related to V_s value of the soil materials.

In Bangladesh, most of the subsurface lithology is characterized by unconsolidated, sandy and clayey floodplain sediments. In alluvial deposits of Bangladesh, following the Srimangal Earthquake in 1918, Great Indian Earthquake in 1897, and the Bengal Earthquake in 1885, the evidences of widespread liquefaction were documented (Middlemiss 1885; Oldham 1899; Stuart 1920; Hossain et al. 2020). In the north and northeast areas of the country, the evidences of liquefaction were observed during paleoseismic studies, which are considered to be triggered by a series of earthquakes along the Dauki fault (Morino et al. 2011, 2014a, b). In addition, the country is sitting close to the tectonically active Himalayan orogenic belt and Arakan megathrust where there are at least five major active fault zones, which have shown evidence of large magnitude earthquakes (Aitchison et al. 2007). Steckler et al. (2016) claimed a locked megathrust exists along the Indo-Burman mountain ranges, which reinforces the notion of the resistance future for major earthquakes. Therefore, it is an absolute necessity for the country to further study the liquefaction resistance evaluation of soils for the major cities.

Rahman et al. (2015) and Rahman and Siddiqua (2017) have conducted liquefaction potential studies for Dhaka, Chittagong, and Sylhet cites in Bangladesh using limited standard penetration test blow count (SPT-N), cone penetration test (CPT), and shear wave velocity (V_s) data. The studies observed that the Holocene alluvium of these cities is susceptible to liquefaction. In those studies, the empirical equations of Youd et al. (2001) were used to calculate the factor of safety (FS) of liquefaction, cyclic resistance ratio (CRR), cyclic stress ratio (CSR), and magnitude scaling factor (MSF). The equations of Iwasaki et al. (1982) were used to calculate liquefaction potential index (LPI). However, in present study, the ANN models were incorporated based on Juang et al. (2003, 2002, 2000) to predict the CRR. The ANN models are inherently bound to produce more realistic results and additional SPT-N and V_s profiles were used to characterize the subsurface heterogeneity with more accuracy. Thus, this study utilizes an improved, robust, and promising method in assessing liquefaction resistance of soils for Dhaka City.

The SPT-N and V_s data from Dhaka City have been used in the assessment of liquefaction resistance of soils for a scenario earthquake of moment magnitude, M_W 7.5 with a peak ground acceleration (PGA) of 0.15 g. According to the proposed Bangladesh Nation Building Code (BNBC), the PGA value for Dhaka City is 0.2 g for the maximum considered earthquake (MCE), which is equivalent to 2% probability of exceedance in 50 years

100 (2475-year return period). The PGA of the design basis earthquake (DBE) is equal to the 2/3 (two-third) of the
101 MCE. Therefore, the PGA of DBE in Dhaka City is 0.13 g. It is observed from historical record of earthquakes that
102 more than M_w 7.0 earthquakes occurred beyond 50 km radius from city center of Dhaka ((Middlemiss 1885; Oldham
103 1899; Stuart 1920). Therefore, the magnitude of earthquake is considered as M_w 7.5 with PGA of 0.15 g in this
104 study.

105 Artificial neural network (ANN) models were used to predict CRR where a variant of performance function
106 (Seed and Idriss 1971, 1982) termed as limit state function (LSF), was considered (Juang et al. 2002, 2000). Firstly,
107 a liquefaction indicator function was formulated for calculating the occurrence of liquefaction. Then, the points at
108 the limit state surface was formulated to determine CRR through simulating the neural network models that were
109 trained using the derived points at the limit state surface by a standard method (Youd et al., 2001). The CSR was
110 estimated on the basis of simplified procedure (Seed and Idriss 1971). The factor of safety (FS) of liquefaction was
111 calculated at selected locations of Dhaka City using estimated CSR and CRR values. Even though the FS may
112 provide an idea of the resistance of soils, it is not enough to represent the state of the liquefaction severity of any
113 location (Sonmez and Gokceoglu 2005). Therefore, the FS values up to the depth of liquefiable layers, which is
114 considered as 20 m depth, were used to determine the LPI of all selected locations of Dhaka City for both datasets
115 (SPT-N and V_s) based on the developed method of Iwasaki et al. (1982) to prepare liquefaction hazard maps for
116 calculating LPI values of the areas where SPT-N and V_s data were not available. For each georgical unit, the
117 liquefaction hazard is also predicted from the cumulative frequency (CF) distribution of the LPI according to Holzer
118 et al. (2006).

119 2. Surface geology of Dhaka City

120 Dhaka City, the capital of Bangladesh, located is on the bank of the Buriganga River, is now one of the world's
121 megacities. The city is encircled by the rivers of Buriganga, Balu, Turag, and Tongi Khal. It occupies an area of
122 about 321 square kilometers with a population of about 14 million. Dhaka City has an average elevation of 6.5 m
123 ranging between 2 and14 m (above the mean sea level) with many depressions (Rahman et al. 2015). Dhaka is
124 situated in the central part of Bangladesh bounded by the Shillong Massif in the north, Precambrian Indian Shield in
125 the west, the Indo-Burman Folded Belt in the east and it is open to the Bay of Bengal in south. Bangladesh covers
126 most part of the Bengal Basin with the maximum sedimentary thickness of 22 km (Alam 1989; Reimann 1993).

Dhaka City is developed partly on the Madhupur Terrace of the Pleistocene age and partly on the low-lying floodplains of the Holocene age. The sediment of the Pleistocene terrace has been deposited on the older floodplains, whereas the Holocene alluvium has been deposited on the recent floodplains of the Ganges-Brahmaputra River Systems (Morgan and McIntire, 1959).

In Dhaka City, six surface geological units have been identified based on the geomorphological, geological, and geotechnical properties. These units are Artificial fill (af), Holocene Alluvial channel deposit (Qhc), Holocene Alluvial valley fill deposit (Qhav), Holocene Alluvium (Qha), Holocene terrace deposit (Qhty), and Pleistocene terrace deposit (Qpty) (Fig. 1) (Rahman et al. 2015).

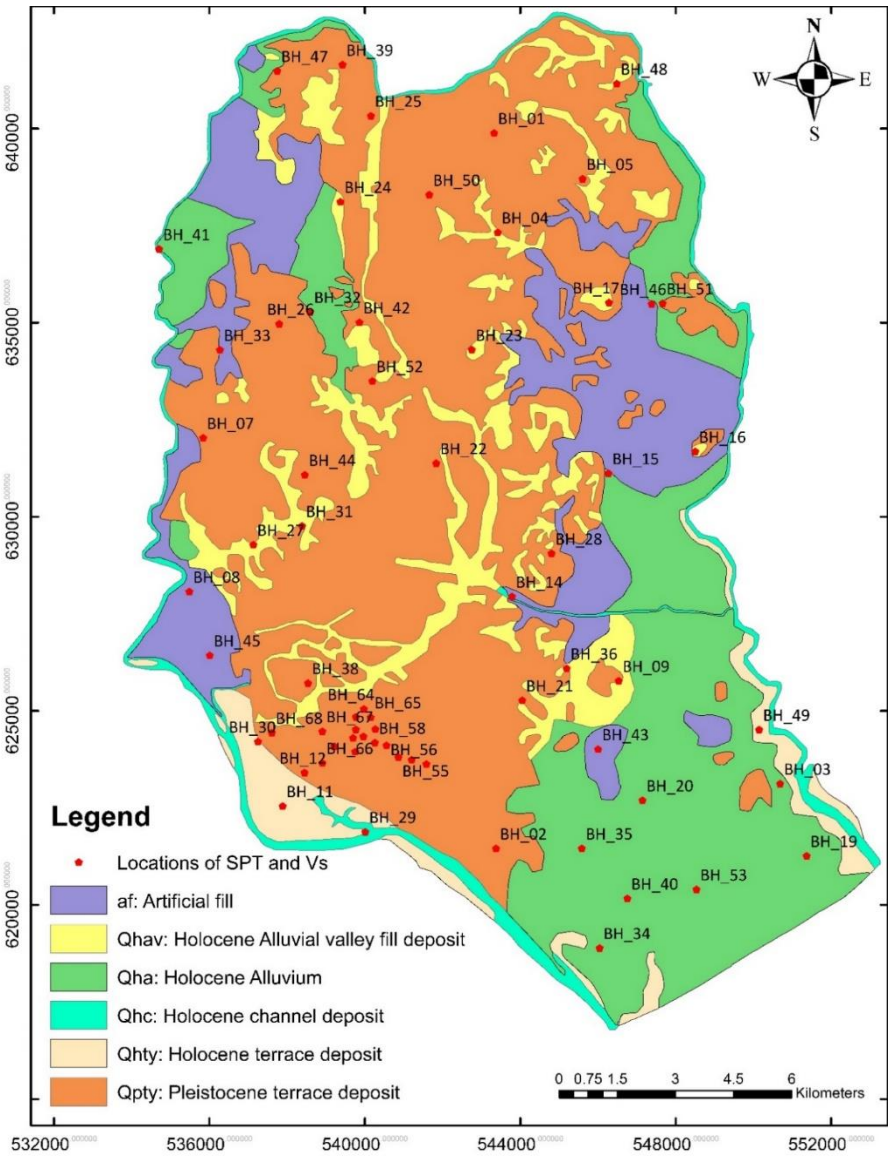

Fig. 1 Surface geological map of Dhaka City with locations of the boreholes (modified from Rahman et al. (2015))

The Pleistocene terrace deposits exposed in the central part of the city are primarily comprised of a 6-8 m thick layer of reddish to yellowish-brown, medium stiff to stiff silty clay that is underlain by a layer of medium dense to very dense silty sand and sand down to the depth of investigation of 20 m. The Holocene alluvium deposits composed of very loose to loose sand, silt, and very soft to soft silty clay are present down to the depth of investigation in northwestern, southeastern, and eastern parts of the city (Rahman et al. 2021). Gray sand, silty sand, and clayey silt make up the artificial fills that are emplaced to the west and east portions of the city. For the

144 emplacement of the artificial fills, both hydraulic dragging from the river and trucks from the land were used, but the
145 ground was not compacted properly during filling, which creates the area prone to liquefaction (Rahman et al.
146 2015).

147 ## 3. Seismotectonics of the region

148 The Bengal Basin is in the northeastern part of the Indian plate and bordering the Indian-Eurasian convergent plate
149 boundary where the Himalayan ranges the north and Indo-Burman ranges in east have been created due to the
150 collision between these plates (Curray et al. 1982; Aitchison et al. 2007). Besides Bangladesh, the Bengal Basin also
151 contains portions of Assam, Tripura, and West Bengal.

152 Dhaka, is seismically vulnerable due to its proximity to the Eurasian and Indian convergent plate boundary
153 (Rahman et al. 2020, 2021). Bangladesh, Myanmar, Nepal, and northeastern India experienced several historical
154 earthquakes (Table 1) that occurred along this plate boundary and associated faults. The Himalayan and the Arakan
155 subduction-collision systems (Fig. 2) also generated many devastating earthquakes in these regions.

156 The Dauki Fault (DF) and the Himalayan Frontal Thrust (HFT) are the main seismotectonic elements of the
157 Himalayan system, while the Arakan subduction-collision system manifests itself through the Indo-Burman Folded
158 Belt along with the megathrust beneath (Steckler et al. 2008; Wang et al. 2014).

159 Bilham and Hough (2006) anticipated that a large earthquake with a magnitude ranging from M_w 7.5 to 8.5
160 may occur in the Himalayan system because of the movement of the Indian plate at a rate of 4 cm/year towards the
161 north and at a rate of 6 cm/year towards the northeast. The 2015 Gorkha Earthquake (M_w 7.8) occurred in Nepal
162 along the subduction interface of the Himalayan System (Goda et al. 2015). It has been revealed by recent
163 paleoseismological investigations that the Dauki fault was activated three times during last thousand years (Yeats et
164 al. 1997; Morino et al. 2011, 2014a) The convergence of the tectonic plates and increasing frequency of earthquakes
165 with large magnitude are, therefore, the indication of active seismic activities in these regions (Rahman and Siddiqua
166 2017).

167

168

169 **Table 1 M**ajor earthquakes that caused damage and casualty in Bangladesh in the last 256 years (Rahman et al.
170 2020)

Date	Earthquake	Moment Magnitude (M_w)	Number of Casualty	Structural Damage
April 2, 1762	Bengal-Arakan Earthquake	8.5[(1)]	500 in Dhaka[(2)]	The earthquake was very strong in Dhaka and Chittagong.[(2)]
July 14, 1885	Bengal Earthquake	6.87[(3)]	Not reported	The highest damage was reported in Sirajganj, Bogra, Jamalpur and Mymensingh. In Dhaka, the damage was very low compared to other areas located at similar distance from the epicenter.[(4)]
June 12, 1897	Great Assam Earthquake	8.03[(3)]	545 in Sylhet[(2)]	The highest damage was reported in Shillong, Assam (India). In Dhaka, almost all masonry buildings were badly damaged, and some were entirely collapsed. In Sylhet, most of the masonry buildings were severely damaged.[(5)]
July 08, 1918	Srimangal Earthquake	7.10[(3)]	Exact numbers were not reported	Most of the tea factories and bungalows at Srimangal (Moulvibazar) were destroyed. Significant damage was reported in Kishoreganj, Sylhet, Habiganj, Agartala (India). In Dhaka, several buildings were slightly cracked.[(6)]

171 Based to [(1)]Wang et al. (2014); [(2)]Banglapedia (accessed on 06 August, 2018); [(3)]Ambraseys and Douglas (2004),
172 [(4)]Middlemiss (1885); [(5)]Oldham (1899); and [(6)]Stuart (1920).

173 ## 4. Material and methods

174 ### 4.1. Database establishment

175 The SPT-N and V_s data from sixty-five (65) boreholes including relevant geotechnical properties of soils were used
176 to assess soil liquefaction resistance of Dhaka City in terms of the FS, which was estimated using the Simplified
177 Procedure of Seed and Idriss (1971). Then, the LPI of each borehole profile was estimated using all FS values of
178 each borehole that were estimated at every 1.5 m interval to a depth of 20 m below the ground surface according to
179 the method introduced by Iwasaki et al. (1978). The borehole sites were selected considering the variation of the
180 geological units in the city (Table 2). The surface geological map (Fig. 1) shows the borehole locations.

181 For training purpose, artificial neural network (ANN) requires the SPT-N and V_s data of the sites where the
182 historical data of liquefaction and non-liquefaction cases are available to find liquefaction indicator (LI) function
183 and points of the limit state function (LSF). The SPT-N data of the historical cases for liquefaction and non-
184 liquefaction were primarily collected by Fear and McRoberts (1995) and later summarized by Idriss and
185 Boulanger (2010). The V_s data were compiled by Andrus et al. (1999). After screening as per the ANN model

applicability criteria of used parameters as described in Juang et al. (2000), total 225 SPT cases (127 cases liquefied) and 225 V_s cases (97 cases liquefied) from 26 earthquakes over 70 sites identified by Andrus et al. (1999) were used for the analysis of the present study.

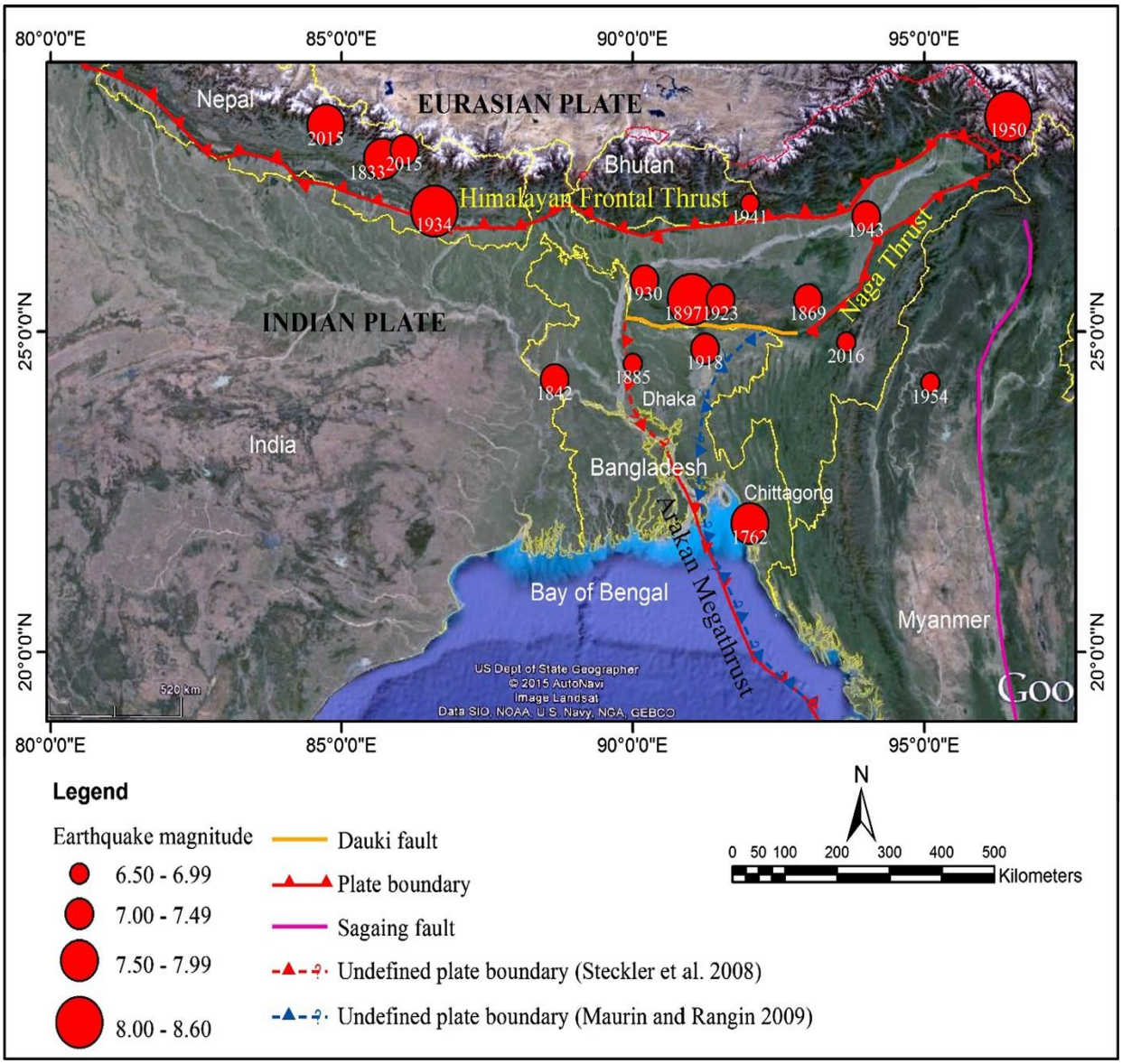

Fig. 2 Recent and historical earthquakes of magnitude greater than M_w 6.5 from 1762 and 2016 (retrieved from Rahman and Siddiqua (2017))

Table 2 Number of boreholes in each surface geological unit of Dhaka City and classes of the geological materials based on the Unified Soil Classification System (USCS)

Geological unit	Number of Boreholes	USCS soil type
Artificial fill (af)	6	SM, SP, MH
Holocene Alluvial valley fill deposits (Qhav)	7	SM, MH, CH
Holocene terrace deposits (Qhty)	4	SM, SP, CL
Holocene channel deposits (Qhc)	0	SM, SP
Holocene Alluvium (Qha)	10	SM, CL, MH, CH
Pleistocene terrace deposits (Qpty)	38	SM, SP, MH, CH, CL

4.2. Factor of safety of liquefaction (FS)

In this study, an updated simplified procedure proposed by Youd et al. (2001)is used in calculating the factor of safety (FS) of liquefaction that is the ratio of the cyclic resistance ratio (CRR) to the cyclic stress ratio (CSR).

4.2.1. Calculation of CSR

The CSR defines the cyclic loading characteristic of soils, by which the seismic demand of the soil layer is determined on a level ground condition. It is the ratio of the cyclic loading-induced average cyclic shear stress to the initial vertical effective stress on the soil particles (Robertson and Campanella, 1985). The following equation of Seed and Idriss (1971) that was slightly adjusted by Juang et al., (2003) has been used to estimate the CSR at z depth from the ground surface due to earthquake loading:

$$CSR_{7.5} = \frac{\tau_{av}}{\sigma'_v} = 0.65\left(\frac{a_{max}}{g}\right)\left(\frac{\sigma_v}{\sigma'_v}\right)r_d/MSF = 0.65.r_d\,.R_p\,.S_L \quad (1)$$

where, $CSR_{7.5}$ = CSR adjusted to an earthquake magnitude of M_w 7.5 using a magnitude scaling factor (MSF); τ_{av} = average cyclic shear stress exerted by an earthquake, σ_v = total vertical stress, σ'_v = effective vertical stress at a depth of question (z); g = gravitational acceleration; a_{max} = peak horizontal ground acceleration (PGA); R_p= overburden pressure ratio (σ_v/σ'_v); S_L= seismic loading parameter (a_{max}/g)/MSF; r_d = stress reduction coefficient represents soil flexibility that depends on z. The calculation formula of r_d according to Youd et al. (2001) is as follows:

$$r_d = \frac{1.000-0.4113z^{0.5}+0.04052z+0.0017532z^{1.5}}{1.000-0.4177z^{0.5}+0.05729z-0.006205z^{1.5}+0.001210z^2} \quad (2)$$

The MSF is the magnitude scaling factor used in liquefaction resistance adjustment to the M_W 7.5 reference magnitude earthquake (Youd et al., 2001).

$$MSF = \left(\frac{Mw}{7.5}\right)^{-2.56} \quad (3)$$

where, M_w= moment magnitude.

4.2.2. Calculation of CRR using ANN

The ability of soil to resist cyclic stress is denoted by the CRR. In the present study, Juang et al. (2000) and Juang et al. (2002) recommended procedures were used for calculating CRR from LSFs derived using the SPT-N and V_s. Initially, the LI function was produced by training with the cases of actual field performance using neural network. The LI function is a trained neural network capable of predicting liquefaction or no liquefaction occurrences with high precision. In general, the LI function (Eq. 4) is a multi-dimensional and highly nonlinear function. It can be developed using a neural network model of three layers:

$$LI = f_T\left[B_0 + \sum_{k=1}^{n}\{W_k f_T(B_{Hk} + \sum_{i=0}^{m} W_{ik}P_i)\}\right] \quad (4)$$

where, B_o refers to the output layer bias (consisting of one neuron only); W_k is the connection weight between k^{th} neuron in the hidden layer and the only one neuron of output layer; B_{Hk} refers to the bias at neuron k (k = 1, n) of the hidden layer; W_{ik} is the connection weight between input variable i (i = 1, m) and the neuron k of the hidden layer.

Secondly, a search mechanism is established using the LI function for searching points at the surface of the limit state. Thirdly, the LSF is specified collectively by the generated points. Finally, neural network models were trained for both datasets (SPT-N and V_s) to determine the CRR for the selected locations of Dhaka City using these generated data points. Conceptually, the LI function of the SPT-N and V_s data may take the following ANN model forms, respectively, as suggested by Juang et al. (2002, 2000):

$$LI_{SPT} = f\left((N_1)_{60}, FCI, \sigma'_v, R_p, S_L\right) \quad (5)$$

$$LI_{Vs} = f\left(V_{s1}, FCI, CSR_{7.5}\right) \quad (6)$$

In this analysis, critical CSR = CRR = f (indices of soil properties) defines the limit state. The LSF, conceptually illustrated in Fig. 3, is defined based on a robust but simple system, was introduced by Juang et al. (2000). For each case in training data, either by increasing normalized soil strength (path B showed in Fig. 3) or by lowering seismic load (path A shown in Fig. 3), the limit state could be reached when liquefaction has been observed. Using path A, as an example, by lowering seismic load while keeping soil resistance unchanged, a new

data pattern is created. With a new input pattern, the LI function would generate a new output. Initially, it is expected that the output would remain the same with a slight lowering of the seismic load. Nonetheless, if this cycle continues to decrease seismic load, ultimately no-liquefaction will be implied by the output. In the given soil condition, the critical load determining the limit state (also called critical CSR), is the upgraded seismic load resulting in a shift in the LI function. Likewise, when any case shows no liquefaction, critical CRR values of the LSF can be generated either by raising the seismic load (path C showed in Fig. 3) or by lowering the value of normalized soil strength parameters (path D showed in Fig. 3). Note that, in some cases, critical CSR searches might not be effective. It occurs when the upper limit of a normal load range is exceeded by seismic load using Path C in Fig. 3 for example. As a result, the liquefaction output of the LI function remains the same.

From each search that would be successful, a data point on the surface of the limit state, which is multidimensional is produced. Since CRR = $CSR_{7.5}$ or critical CRR defines the limit state boundary surface by its definition, an LSF is defined through CRR= *f* (indices of soil properties) once enough data points were obtained. Fig. 4 illustrates the described searching mechanism.

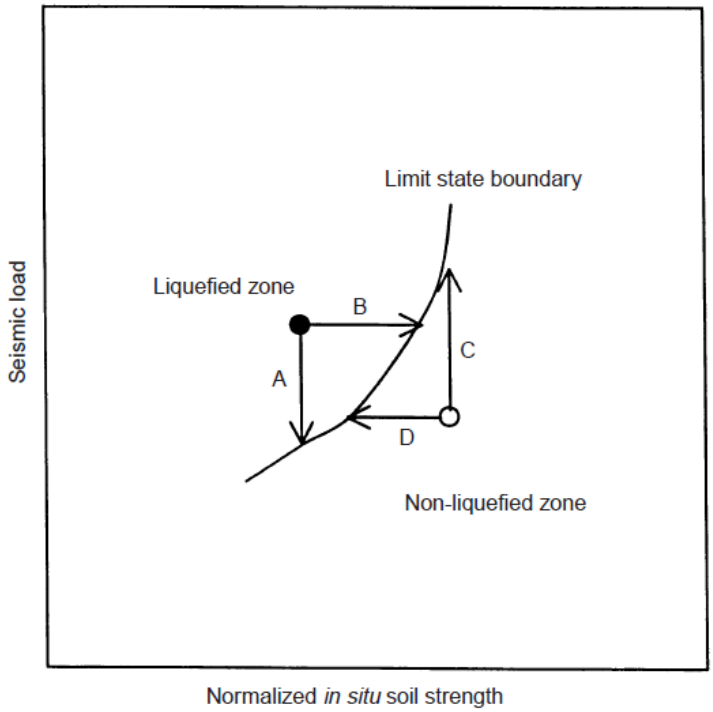

Fig. 3 Conceptual model of the mechanism to search limit state boundary (after Chen and Juang, (2000))

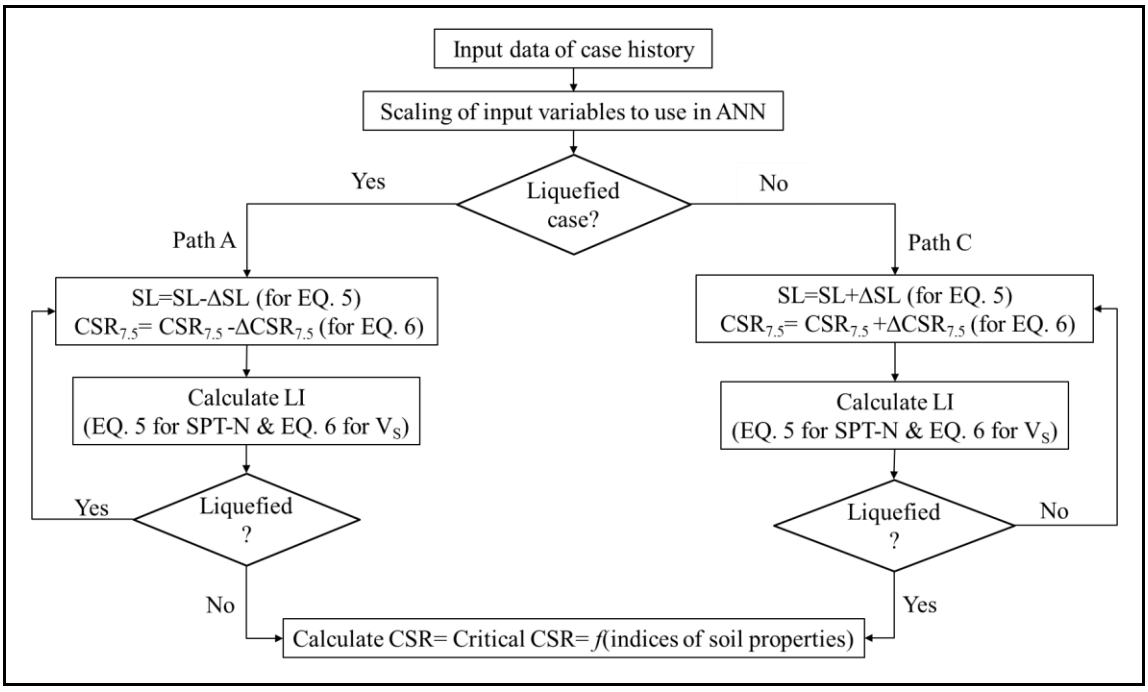

Fig. 4 Searching mechanism of critical cyclic stress ratio (CSR) (after Juang et al. (2000))

After generating the boundary surface points based on the algorithm mentioned above, by training those points with a feed-forward, three-layer neural network, connection weights and biases can be produced, that would then be used in CRR estimation:

$$CRR = f_T\left[B_0 + \sum_{k=1}^{n}\{W_k f_T(B_{Hk} + \sum_{i=0}^{m} W_{ik}P_i)\}\right] \quad (7)$$

This equation is the same as Equation 4.

Conceptually, the LSF from the SPT-N and V_s data may take the following ANN model forms, respectively, as suggested by Juang et al. (2002, 2000):

$$CRR_{SPT} = f\left((N_1)_{60}, FCI, \sigma'_v, R_p\right) \quad (8)$$

$$CRR_{Vs} = f\left(V_{s1}, FCI\right) \quad (9)$$

Table 3 and Table 4 show all specifications of the ANN model for training that were implemented using the neural network toolbox of MATLAB for LI and LSFs, respectively. MATLAB offers an immersive computational platform with numerous built-in algorithms, along with a programming language. It provides a network neural

toolbox containing source code for all such algorithms for training neural networks including the LM algorithm (Levenberg-Marquardt) that could be adjusted according to the circumstances provided (Beale et al. 2017).

Table 3 Specifications for artificial neural network (ANN) models of liquefaction indicator (LI) and limit state functions (LSFs)

Network Type	Training Function (both hidden and output layers)	Transfer Function	Adaption Learning Function	Performance Function
Feed-forward Backpropagation	Levenberg-Marquardt (TRAINLM)	Hyperbolic Tangent Sigmoid (tansig)	Gradient descent with momentum (LEARNGDM)	Mean squared error (MSE)

Table 4 Numbers of layers and hidden neurons in artificial neural network (ANN) model of liquefaction indicator (LI) and limit state functions (LSFs)

	LI_{SPT}	LI_{Vs}	CRR_{SPT}	CRR_{Vs}
Number of layers	3	3	3	3
Number of hidden neurons	8	6	5	4

4.2.3. Calculation of FS

The FS was calculated using Eq. 10 from the CSR, CRR, and MSF for earthquake magnitude other than M_w 7.5. The CSR was calculated for all data points of two datasets (SPT-N and V_s) using Eq. 1 and the CRR was predicted from the simulating normalized data (SPT-N and V_s) of Dhaka City using the developed ANN models of LSF.

$$F_S = \left(\frac{CRR_{7.5}}{CSR}\right) MSF \quad (10)$$

If FS ≤ 1 it is considered that liquefaction occurs; and if FS > 1 liquefaction is not likely to occur.

4.3. LPI Calculation

The calculation of the LPI uses the FS derived from the CRR and CSR. Iwasaki et al. (1978) suggested the LPI, which can be estimated using the FS values calculated from the SPT-N, V_s, and CPT over the top 20 m, as follows:

$$LPI = \int_0^{20} F(z)W(z)\,dz \quad (11)$$

where, $W(z) = \begin{cases} 10 - 0.5z; & z < 20m \\ 0 & ; \ z > 20m \end{cases}$; z = Depth in meters

and $F(z) = \begin{cases} 1 - FS; & FS < 1.0 \\ 0 & ; \ FS \geq 1.0 \end{cases}$

293 Iwasaki et al. (1982) mentioned that, if the LPI of a site is greater than 15, it is highly prone to severe
294 liquefaction and if the LPI of any site is lower than 5, the liquefaction is not expected to show surface manifestation.

295 ## 5. Results

296 Based on the approach discussed above, initially using 225 field performance cases (85% for training and 15% for
297 testing) for the SPT-N and V_s were used separately to train the LI function for each data set. One of the most
298 effective ways to assess the ANN model efficiency is by observing the coefficient of determination (R) value. In the
299 case of the ANN model for the LI function, the R-value for the SPT-N data training was 0.886 and testing 0.92, and
300 the R values for the V_s data training and testing were 0.89. Next, points were generated in the limit state boundary
301 with the help of the respective LI functions for different datasets using the searching mechanism shown in Fig. 4.

302 From the searching, total of 143 and 236 points have been generated for the SPT-N and V_s datasets,
303 respectively, on the limit state surface. Then, to approximate the LSF for the respective datasets (Eqs. 8 and 9), these
304 data points were then used in training neural networks. The trained neural networks approximate the unknown but
305 real functional relation between the output (CRR) and the inputs (indices of soil properties). Plotting the output
306 values from training against the actual field performance value (or targeted value) also shows the performance of an
307 ANN model. Fig. 5 and Fig. 6 show such plots for the training and testing according to Eqs. 8 and 9 of generated
308 data points at limit state surface from the SPT-N and V_s data. Table 6 and Table 7 are showing the weights and
309 biases of connections obtained the trained ANN models for SPT-N and V_s data, respectively.

310 The FS values were calculated from the CSR and CRR values that were derived from simulating trained
311 ANN models for the LSF using normalized parameters (as in Eqs. 8 and 9) of each location. The LPI values were
312 calculated using Eq. 11 from the FS of the SPT-N and V_s datasets are shown in Table 8.

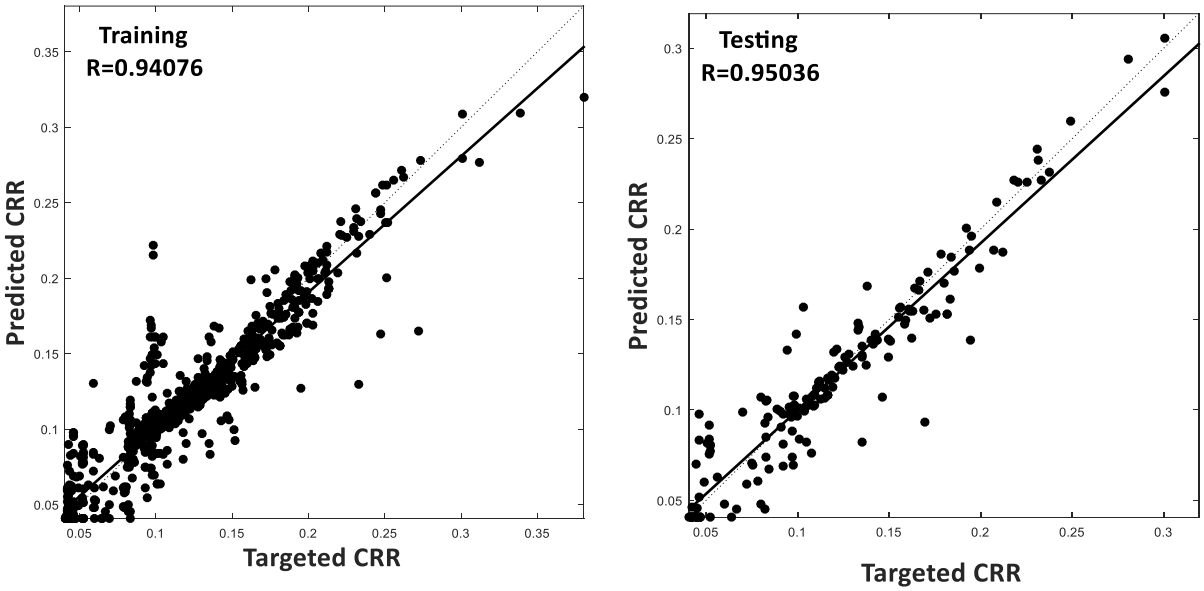

313

314 **Fig. 5** Performance of CRR_{SPT} model

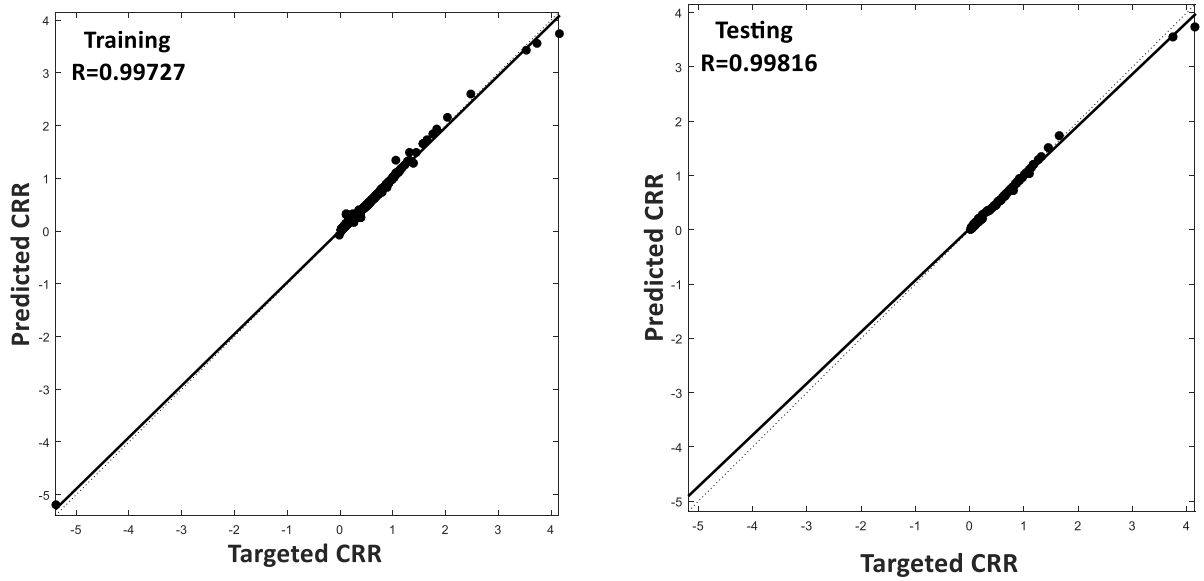

315

316 **Fig. 6** Performance of CRR_{Vs} model

317

318

319

320

321

322

323

324

Table 6 Weights and biases of connections in CRR_{SPT}

Hidden neuron (HN) no.	Weight					Bias	
	W_{ik}				W_k	B_k	B_o
	Input 1 (i=1)	Input 2 (i=2)	Input 3 (i=3)	Input 4 (i=4)	Output neuron	Hidden layer	Output layer
HN1 (k=1)	-1.9681	1.2399	0.93542	-0.71182	-36.1196	1.8671	-46.7613
HN2 (k=2)	0.52733	0.94369	-1.2764	1.735	20.171	-0.53251	
HN 3 (k=3)	-1.663	0.98884	1.0491	-0.56474	82.5362	2.175	
HN4 (k=4)	-4.7013	-2.7607	30.4863	-44.1878	0.28948	-33.1536	
HN5 (k=5)	0.42838	0.93002	-1.2782	1.7321	-20.1837	-0.60614	

Table 7 Weights and biases of connections in CRR_{Vs}

Hidden neuron (HN) no.	Weight			Bias	
	W_{ik}		W_k	B_k	B_o
	Input 1 (i=1)	Input 2 (i=2)	Output neuron	Hidden layer	Output layer
HN1 (k=1)	1.1607	0.032301	16.9411	-2.7486	17.0539
HN2 (k=2)	-119.0633	-5.0242	-21.8624	-29.4215	
HN3 (k=3)	109.4112	4.7075	16.1528	27.7892	
HN4 (k=4)	106.6118	4.5549	-38.0221	26.6818	

342 **Table 8** The SPT-N and V_s based LPI values of each borehole for a scenario earthquake of Mw 7.5 with a PGA of
343 0.15 g. At each borehole, the SPT-N value and Vs measurement were taken at each 1.5 m interval down to a depth
344 21 m.

Borehole No.	Coordinates		Geomorphological Unit	Unit Symbol	Depth of GWT (m)	LPI from SPT-N	LPI from V_s
	Easting	Northing					
BH-01	543326.921	639885.898	Lower Madhupur Terrace	Qpty	7.0	0.00	0.00
BH-02	543376.105	621458.48	Upper Madhupur Terrace	Qpty	5.0	0.00	0.00
BH-03	550687.573	623127.326	Flood Plain	Qha	3.0	11.94	19.19
BH-04	543419.417	637327.45	Deep Alluvial Gully	Qhav	5.0	12.76	16.11
BH-05	545603.314	638709.462	Lower Madhupur Terrace	Qpty	3.0	0.00	0.00
BH-07	535839.846	632035.635	Upper Madhupur Terrace	Qpty	18.0	0.00	0.00
BH-08	535484.452	628074.969	Swamp/ Depression	af	4.0	8.93	2.49
BH-09	546532.2	625777.363	Upper Madhupur Terrace	Qpty	4.5	0.00	0.00
BH-11	537885.386	622550.343	Point Bar	Qhty	4.5	12.76	0.00
BH-12	538449.42	623412.903	Upper Madhupur Terrace	Qpty	5.5	4.46	0.00
BH-13	539212.062	624091.499	Upper Madhupur Terrace	Qpty	1.5	2.34	0.34
BH-14	543787.064	627948.675	Deep Alluvial Gully	af	1.5	19.99	13.57
BH-15	546267.801	631123.967	Swamp/ Depression	Qha	1.5	9.79	7.78
BH-16	548501.53	631684.808	Upper Madhupur Terrace	Qhav	4.5	2.79	9.95
BH-17	546282.102	635521.81	Lower Madhupur Terrace	Qhav	1.5	23.08	17.16
BH-19	551367.994	621269.109	Flood Plain	Qha	4.0	6.66	16.73
BH-20	547143.988	622700.284	Flood Plain	Qha	1.5	0.00	0.00
BH-21	544049.881	625273.913	Upper Madhupur Terrace	Qpty	6.0	0.00	0.00
BH-22	541835.945	631382.021	Upper Madhupur Terrace	Qpty	2.0	9.10	0.00
BH-23	542752.243	634307.125	Shallow Alluvial Gully	Qhav	2.5	1.30	2.89
BH-24	539372.339	638115.516	Shallow Alluvial Gully	Qhav	3.0	2.38	0.69
BH-25	540158.18	640331.941	Upper Madhupur Terrace	Qpty	4.0	6.39	0.00
BH-26	537796.56	634974.463	Shallow Alluvial Gully	Qpty	4.0	3.54	0.00
BH-27	537132.08	629283.366	Deep Alluvial Gully	Qhav	3.5	6.56	11.65
BH-28	544802.623	629058.89	Lower Madhupur Terrace	Qpty	3.0	0.67	1.03
BH-29	540012.645	621887.187	Point Bar	Qhty	6.7	0.00	0.00
BH-30	537251.312	624212.582	Point Bar	Qhty	5.5	0.00	2.46
BH-31	538385.375	629766.609	Upper Madhupur Terrace	Qpty	4.0	2.93	0.00
BH-32	538594.907	635280.65	Swamp/ Depression	Qha	1.5	20.70	21.10
BH-33	536272.23	634302.618	Madhupur Slope	af	1.8	19.36	21.13
BH-34	546042.619	618894.671	Flood Plain	Qha	1.5	11.96	3.23
BH-35	545583.954	621460.646	Flood Plain	Qha	3.7	4.53	4.43
BH-36	545193.435	626097.174	Deep Alluvial Gully	Qhav	1.5	20.86	18.98
BH-37	541583.654	623635.279	Upper Madhupur Terrace	Qpty	3.7	3.84	6.12
BH-38	538537.681	625718.273	Upper Madhupur Terrace	Qpty	2.3	3.10	0.00
BH-39	539424.733	641648.101	Upper Madhupur Terrace	Qpty	1.5	1.00	0.00
BH-40	546755.248	620173.641	Flood Plain	Qha	1.5	0.08	0.00
BH-41	534707.013	636900.28	Back Swamp	Qha	1.5	17.63	7.45
BH-42	539861.822	635008.868	Lower Madhupur Terrace	Qpty	2.1	2.76	0.00
BH-43	546001.183	624015.105	Swamp/ Depression	af	2.7	18.69	18.00
BH-44	538455.075	631081.218	Upper Madhupur Terrace	Qpty	1.5	0.50	0.00
BH-45	536010.634	626431.552	Back Swamp	af	2.5	3.63	0.00
BH-46	547379.066	635489.77	Swamp/ Depression	af	1.5	16.11	19.57
BH-47	537745.941	641488.616	Upper Madhupur Terrace	Qpty	1.5	1.21	0.00
BH-48	546481.069	641160.514	Lower Madhupur Terrace	Qpty	1.5	1.95	4.77
BH-49	550146.733	624520.859	Natural Levee	Qhty	2.4	14.19	0.00
BH-50	541657.054	638301.25	Upper Madhupur Terrace	Qpty	1.5	0.00	0.00
BH-51	547661.889	635503.001	Lower Madhupur Terrace	Qpty	2.3	6.47	0.00
BH-52	540194.154	633499.907	Deep Alluvial Gully	Qpty	15	0.00	0.00

BH-53	548533.3280	620405.1820	Swamp/ Depression	Qha	3.0	3.07	0.00
BH-54	541203.9604	623742.6556	Upper Madhupur Terrace	Qpty	2.27	0.00	0.00
BH-55	540863.6783	623812.5430	Upper Madhupur Terrace	Qpty	3.05	0.00	0.00
BH-56	540556.7901	624114.3428	Upper Madhupur Terrace	Qpty	2.74	0.00	0.00
BH-57	540271.1999	624531.2280	Upper Madhupur Terrace	Qpty	4.72	0.00	0.00
BH-58	540259.4230	624184.6964	Upper Madhupur Terrace	Qpty	4.27	0.00	0.00
BH-59	539964.3541	624346.7240	Upper Madhupur Terrace	Qpty	4.27	0.00	0.00
BH-60	539751.2216	623952.3698	Upper Madhupur Terrace	Qpty	3.36	0.00	0.00
BH-61	539696.5425	624307.4642	Upper Madhupur Terrace	Qpty	1.98	0.00	0.00
BH-62	539769.1142	624526.0790	Upper Madhupur Terrace	Qpty	2.59	0.00	0.00
BH-63	539771.9987	624849.2276	Upper Madhupur Terrace	Qpty	3.36	0.00	0.00
BH-64	539976.2721	625051.2678	Upper Madhupur Terrace	Qpty	3.36	0.00	0.00
BH-65	540148.5704	624838.1984	Upper Madhupur Terrace	Qpty	3.81	0.00	0.00
BH-66	538908.2739	623661.4842	Upper Madhupur Terrace	Qpty	3.05	0.00	0.00
BH-67	538906.2905	624477.1336	Upper Madhupur Terrace	Qpty	8.23	0.00	0.00
BH-68	537608.7915	624440.5012	Upper Madhupur Terrace	Qpty	4.57	0.00	0.00

The surface geological units of Dhaka City is divided into three liquefaction hazard zones based on the LPI values (Table 9). For each zone, the cumulative frequency (CF) distributions of the LPI values of the SPT-N and V_s data are shown in Fig. 7 and Fig. 8, respectively.

Table 9 Liquefaction hazard zones along with their respective number of SPT-N and V_S profiles

Zone	Geological units	Number of SPT-N and V_S profiles
Zone 1	Pleistocene terrace deposit	38
Zone 2	Holocene terrace deposit Holocene and Alluvial valley fill deposit	11
Zone 3	Holocene Alluvium and Artificial fill	16

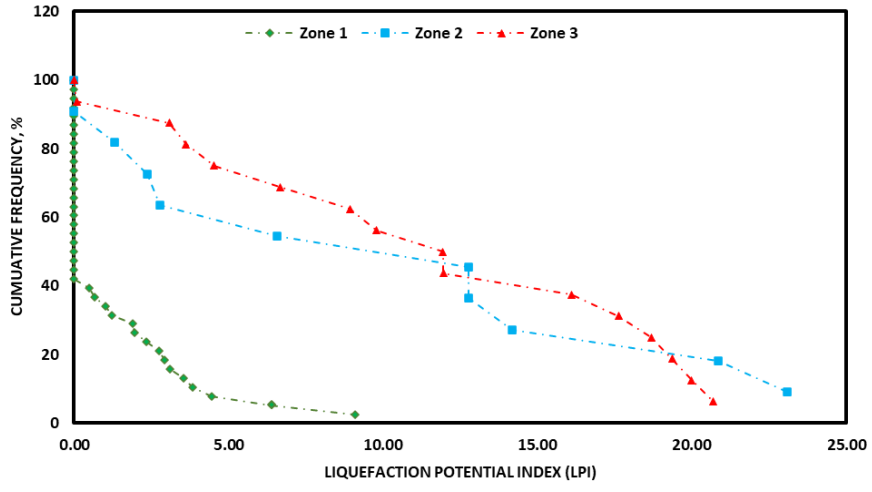

Fig. 7 Cumulative frequency (CF) distribution of LPI values of SPT-N data for each liquefaction hazard zone of Dhaka City

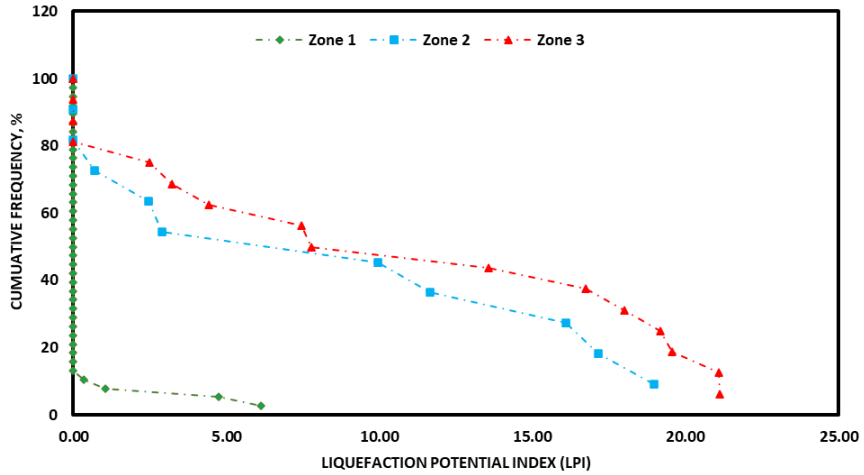

Fig. 8 Cumulative frequency (CF) distribution of LPI values of Vs data for each liquefaction hazard zone of Dhaka City

The LPI values of sixty-five (65) borehole profiles along with the contour of LPI values (0, 5, 10, 15, and 20) are shown on the maps to visualize the spatial distribution of liquefaction severity in the city (Fig. 9 and Fig. 10). One the basis of the LPI values, the liquefaction hazard of different areas of Dhaka City is classified according Iwasaki et al. (1982) (Table 10)

Liquefaction hazard of each surface geological unit was also classified by the cumulative frequency (CF) distribution at the LPI value of 5, which can be used to define the threshold for observing liquefaction surface effects (Holzer et al. 2006). The map of the SPT-N data shows that 15%, 53%, and 69% areas, whereas the map of the V_s data shows that 11%, 48%, and 62% of areas of Zone 1, Zone 2, and Zone 3, respectively, will exibit liquefaction surface effects.

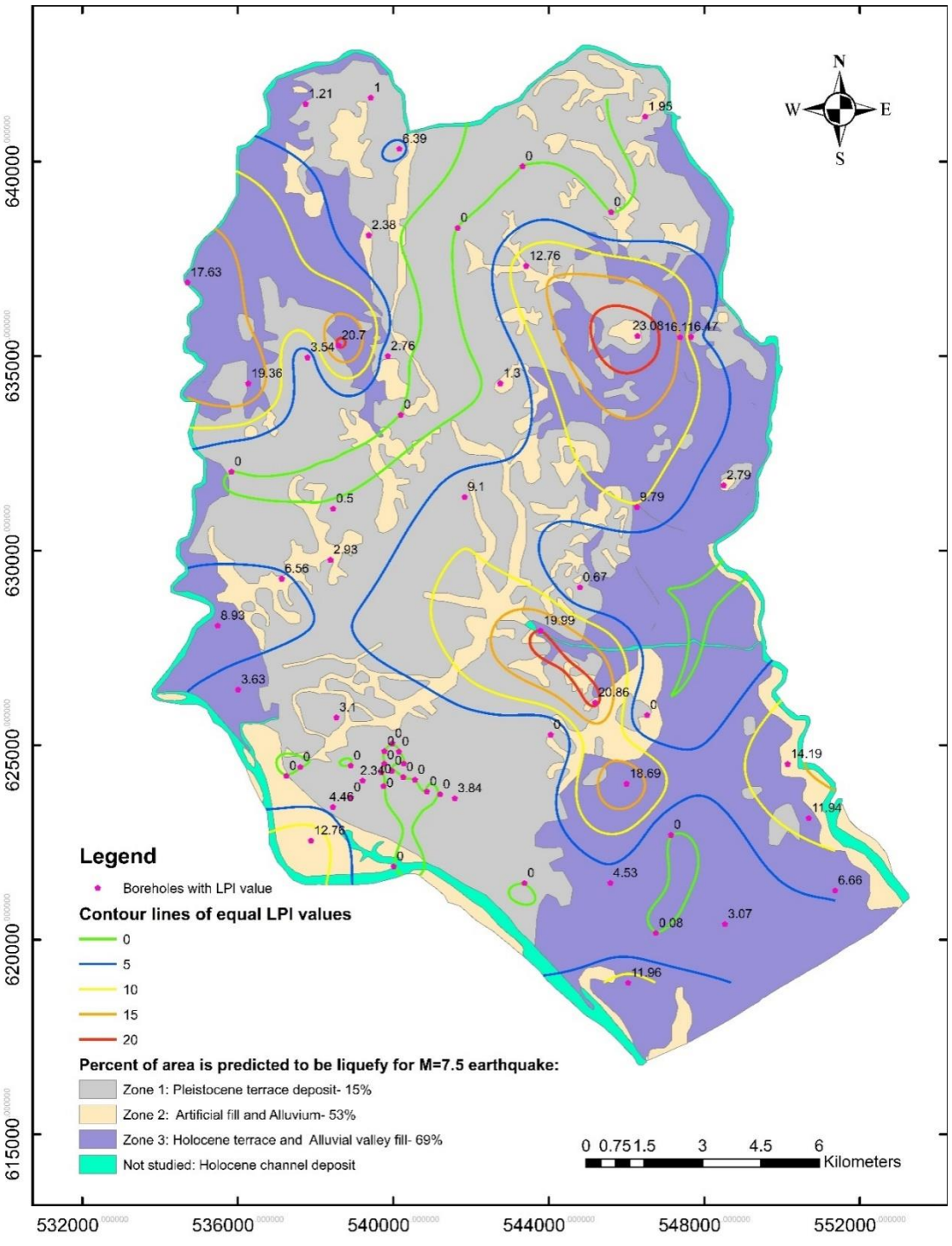

Fig. 9 Liquefaction hazard map for Dhaka City using the LPI values of the SPT-N data for a scenario earthquake of Mw 7.5 with a peak horizontal ground acceleration (PGA) of 0.15 g. According to Iwasaki et al. (1982), liquefaction hazard for LPI > 15 is very high, for 5 < LPI≤ 15 is high, for 0 <LPI ≤ 5 is low; and for LPI = 0 is very low. According to Holzer et al. (2006), the cumulative frequency (CF) distributions of the LPI of three zones indicate that 15%, 53%, and 69% of areas of Zone 1, 2, and 3, respectively, exhibit surface manifestation of liquefaction

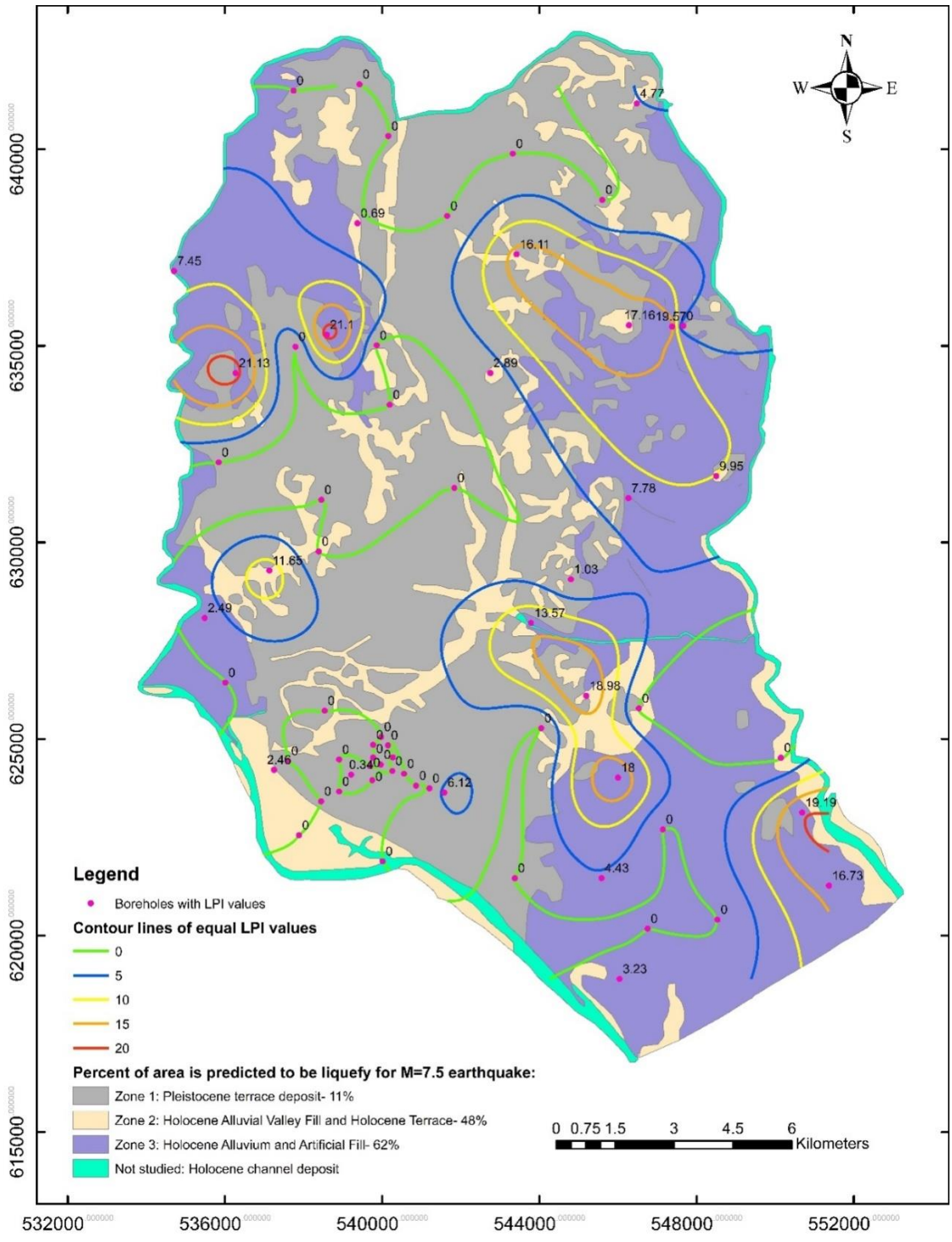

Fig. 10 Liquefaction hazard map for Dhaka City using the LPI values of the Vs data for a scenario earthquake of Mw 7.5 with a peak horizontal ground acceleration (PGA) of 0.15 g. According to Iwasaki et al. (1982), liquefaction hazard for LPI > 15 is very high, for 5 < LPI≤ 15 is high, for 0 <LPI ≤ 5 is low; and for LPI = 0 is very low. According to Holzer et al. (2006), the cumulative frequency (CF) distributions of the LPI of three zones indicate that 15%, 53%, and 69% of areas of Zone 1, 2, and 3, respectively, exhibit surface manifestation of liquefaction

Table 10 Classes of liquefaction hazard on the basis of LPI values (after Iwasaki et al. (1982))

LPI	Liquefaction hazard
LPI > 15	Very High
5 < LPI ≤ 15	High
0 < LPI ≤ 5	Low
LPI = 0	Very low

A comparison between the LPI values derived from the SPT-N and V_s is illustrated in Fig. 11. In most of the cases, the LPI values of the SPT-N data are higher than that of the V_s data.

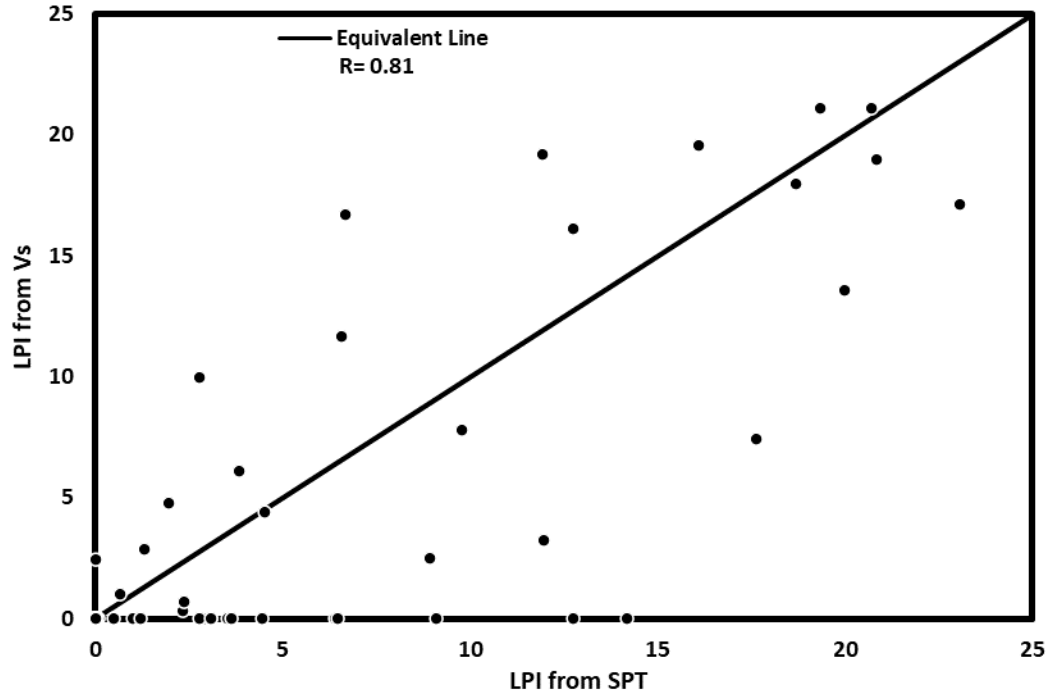

Fig. 11 Comparison between LPI values of SPT-N and Vs datasets

6. Discussion

The liquefaction hazard map offers an opportunity to quantitatively estimate the liquefaction susceptibility of Dhaka City. The spatial liquefaction potential was determined by calculating the LPI values from the liquefaction FS estimated from both SPT-N and V_s at each 1.5 m interval of a borehole down to a depth of 20 m. The contour lines of equal LPI values were drawn to represent the LPI values of the locations where there was no borehole. Three

liquefaction hazard zones were identified in the city based on the CF distribution of LPI of each geological unit to determine the percentage of the area of these zones that are likely to liquefy in a defined scenario earthquake.

In Zone 1, up to 6 - 8 m depth is formed of stiff to hard, reddish- to yellowish-brown Pleistocene clayey soils that is underlain by the medium to very dense, yellowish-brown Plio-Pleistocene sandy soils up to the depth of investigation of 20 m. In the case of the SPT-N data, the liquefaction potential in Zone 1 ranges from low to very low with the LPI values from 0 to 4.46, except boreholes BH-22 and BH-25 with the LPI values of 9.10 and 6.39, respectively. The cumulative frequency (CF) distribution of the SPT-N based LPI values of Zone 1 suggests that fifteen percent (15%) of the area of this zone would have liquefaction surface effects (Fig. 9). For the V_s data, the liquefaction potential in Zone 1 is also from very low to low with the LPI values from 0 to 4.77, except boreholesBH-37 with the LPI value of 6.12. The CF distribution of the V_s based LPI values of Zone 1 suggests that eleven percent (11%) of the area of this zone would have liquefaction surface effects (Fig. 10). In case of outliers, the SPT-N based LPI values of boreholes BH-22 and BH-25 are 9.10 and 6.39, respectively, but the V_s based LPI values are 0 for both boreholes, which seems more accurate as these two boreholes are in the Pleistocene terrace (Madhupur terrace)that is not likely to liquefy. On the other hand, at borehole BH-37, the V_s based LPI value is 6.12 while SPT-N based LPI is 3.84 and it is also in the Pleistocene terrace, therefore, the LPI value of 3.84 from the SPT-N data seems more accurate.

Zone 2 includes the Holocene terrace deposits and alluvial valley fill where the terrace deposits are formed of sandy and silty gray soils which include point and channel bars and natural levees of the existing rivers. The valley-fill deposits that have been deposited in the depressions and valleys of the Pleistocene terrace, are comprised of gray sandy soils and gray to dark gray clayey soils. In Zone 2, the SPT-N based LPI values range from 0 to 23.08,which imply a range of no potential to very high potential of liquefaction. The surface effects of liquefaction will be exhibited in fifty-three percent (53%) area of Zone 2. The V_s based LPI values are from 0 to 18.98, which also imply a range of no potential to very high potential of liquefaction in Zone 2. The surface effects of liquefaction will be exhibited in forty-eight percent (48%) area of this zone. At boreholesBH-11 and BH-49 of this zone, the SPT based LPI values are 12.76 and 14.19, respectively, whereas the V_s based LPI values are 0 at these boreholes. BH-11 is located on point bar and BH-49 is on the natural levee and both are usually more prone to liquefaction. Therefore, the SPT-N provides a more accurate result in this case.

Zone 3 contains artificial fills and Holocene alluvium that are comprised of gray sandy and clayey soils. The SPT-N based LPI values of this zone vary from 0 to 20.70, which indicate a range of no potential to very high potential of liquefaction. The CF distribution of the SPT-N based LPI values suggest that the surface effects of liquefaction will be exhibited in sixty-nine percent (69%) area of this zone. The V_s based LPI values of this zone range from 0 and 21.13, which also indicate a range of no potential to very high potential of liquefaction. The CF distribution of the V_s based LPI values suggest that the surface effects of liquefaction would be exhibited in sixty-two percent (62%) area of this zone. In case of Zone 3, the SPT-N based LPI values of boreholesBH-8, BH-19, BH-34, and BH-41 are 8.93, 6.66, 11.96, and 17.63, respectively, whereas the V_s based LPI values of these boreholes are 2.49, 16.73, 3.23, and 7.45. Borehole BH-8 is in the swamp, so the SPT-N based LPI value (8.93) appears more reliable. Borehole BH-34 is in a floodplain, which is more likely to have an LPI value of more than 5, therefore, the SPT-N based LPI value (11.96) appears more reliable than the V_s based LPI (3.23) value. Borehole BH-19 and BH-41 are in the floodplain and back swamp, respectively, and in both cases for both datasets their LPI values are greater than 5, but it cannot be reliably said either of these will be greater than 15 or not as the output differs.

From the historical earthquake records of Bangladesh, it was observed that liquefaction occurred in silty and sandy alluvium of the Holocene floodplains during the 1885 Bengal earthquake (M_w 6.87), 1897 Great Assam earthquake (M_w 8.03), and 1918 Srimangal earthquake (M_w 7.2) (Middlemiss 1885; Oldham 1899; Stuart 1920). The results of the present study also suggest that severe liquefaction may occur in the silty and sandy alluvium of the Holocene floodplains and the Pleistocene terrace deposits are not likely to liquefy during an earthquake of M_w 7.5 having a PGA of 0.15 g. It can also be mentioned that during the 1995 Kobe earthquake in Japan, severe liquefication occurred in loose fills (Hamada et al. 1995). Holzer et al. (2006) have also identified that the Pleistocene deposits have low liquefaction potential and the artificial fills and alluvium have high liquefaction potential.

7. Conclusions

In this study, both SPT-N and V_s data have been used to calculate the LPI for the preparation of liquefaction hazard maps of Dhaka City using simplified procedure considering a scenario earthquake of M_W 7.5 with a PGA of 0.15 g. In the present study, ANN model has been used to predict the CRR from the SPT-N and V_s data, as it provides more realistic and reliable results using sufficient actual field performance cases. From the results, it is noted that the SPT-

446 N based LPI value is higher than the V_s based LPI value at most of the boreholes. Three liquefaction hazard zones
447 are identified in the city based on the CF distribution of the LPI of each geological unit and the LPI contour lines 0,
448 5, 10, 15, and 20 have been drawn to demonstrate spatial distribution of liquefaction hazard in the city.

449 The map of the SPT-N based LPI values indicates that 15%, 53%, and 69% areas, whereas the map of the
450 V_s based LPI values indicates that 11%, 48%, and 62% areas of Zone 1, 2, and 3 exhibit surface manifestation of
451 liquefaction for a scenario earthquake of M_w 7.5 with a PGA of 0.15 g. Therefore, it can be concluded that the CF
452 distribution of the LPI of both SPT-N and V_s data show almost similar severity of liquefaction in Zone 1, 2, and 3.

453 The uncertainties associated with the calculation of the LPI can be reduced by using more SPT-N, V_s data,
454 variation in groundwater level, accurate surface geological unit boundary delineation, and appropriate ground
455 motion. Finally, this liquefaction hazard map of Dhaka City can be used as a guide for future urban development and
456 planning to reduce the liquefaction associated damages and loss.

457 **Acknowledgments**

458 The authors would like to thank the Comprehensive Disaster Management Programme(CDMP), Department of
459 Disaster Science and Management (DSM), University of Dhaka, Bangladesh for providing the support to collect the
460 data of this research. The authors are also thankful to the University of Dhaka for allowing them to conduct this
461 research.

462 **Authors' contribution**

463 ASMMK and AKFF initiated the study and carried out literature review. AKFF and MSH tested and interpreted the
464 data. ASMMK, MJR, AKFF drafted the manuscript and ASMMK supervised the whole work. Finally, all Authors
465 read, critically reviewed, and approved the final version of the paper.

466 **Ethical considerations**

467 Not applicable.

468 **Availability of data and materials**

469 Data set used in this study is available at

470 **Conflict of Interest**

471 Authors have no conflict of interest.

472 **Funding source**

This research has no funds.

Informed consent

Not applicable for this study.

References

Aitchison JC, Ali JR, Davis AM (2007) When and where did India and Asia collide? Journal of Geophysical Research 112:1978–2012

Alam M (1989) Geology and depositional history of Cenozoic sediments of the Bengal Basin of Bangladesh. Palaeogeography, Palaeoclimatology, Palaeoecology 69:125–139. doi: 10.1016/0031-0182(89)90159-4

Ambraseys NN, Douglas J (2004) Magnitude calibration of north Indian earthquakes. Geophysical Journal International 159:165–206. doi: 10.1111/j.1365-246X.2004.02323.x

Andrus BRD, Member A, Ii KHS (2000) Liquefaction resistance of soils from shear-wave velocity. Journal of Geotechnical and Geoenvironmental Engineering 126:1015–1025

Andrus RD, Stokoe KH (1997) Liquefaction resistance based on shear wave velocity. In: Proceeding of NCEER workshop on evaluation of liquefaction resistance of soils. National Center for Earthquake Engineering Research, Sate University of New York, Buffalo, pp 89–128

Andrus RD, Stokoe KH, Chung RM (1999) NISTIR6277 Draft Guidelines for Evaluating Liquefaction Resistance Using Shear Wave Velocity Measurements and Simplified Procedures

Beale MH, Hagan MT, Demuth HB (2017) Neural Network Toolbox TM User's Guide.

Castro G (1969) Liquefaction of Sands. PhD Thesis. Harvard University, Cambridge.

Castro G, Poulos SJ (1977) Factors affecting liquefaction and cyclic mobility. J Geotech Engng Div 103:501–516

Castro G, Poulos SJ, France JW, Enos JL (1982) Liquefaction induced by cyclic loading. Report by Geotechnical Engineers, Inc., to the National Science Foundation, Washington, D.C

Chao SJ, Hsu HM, Hwang H (2010) Soil liquefaction potential in Ilan City and Lotung Town, Taiwan. Journal of

GeoEngineering 5:21–27. doi: 10.6310/jog.2010.5(1).3

Chen CJ, Juang CH (2000) Calibration of SPT- and CPT-based liquefaction evaluation methods. In: Mayne P, Hryciw R (eds) Innovations and applications in geotechnical site characterization. 97, Geotechnical special publication, ASCE, Reston, pp 49–64

Curray JR, Emmel FJ, Moore DG, Raitt RW (1982) Structure, tectonics, and geological history of the northeastern Indian Ocean. In: The ocean basins and margins. Springer, pp 399–450

Fear CE, McRoberts EC (1995) Report on liquefaction potential and catalogue of case records. Internal Res. Rep., Dept. of Civil Engineering, Univ. of Alberta, Edmonton, Alberta, Canada

Goda K, Kiyota T, Pokhrel RM, et al (2015) The 2015 Gorkha Nepal earthquake: Insights from earthquake damage survey. Frontiers in Built Environment 1:1–15. doi: 10.3389/fbuil.2015.00008

Hamada M, Isoyama R, Wakamatsu K (1995) The 1995 Hyogoken-Nanbu Kobe earthquake-Liquefaction, ground displacement, and soil condition in the Hanshin area. The School of Science and Engineering, Waseda University, Tokyo

Holzer TL, Bennett MJ, Noce TE, et al (2006) Liquefaction hazard mapping with LPI in the greater Oakland, California, area. Earthquake Spectra 22:693–708

Hossain MS, Kamal ASMM, Rahman MZ, et al (2020) Assessment of soil liquefaction potential: a case study for Moulvibazar town, Sylhet, Bangladesh. SN Applied Sciences 2:. doi: 10.1007/s42452-020-2582-x

Idriss IM, Boulanger RW (2004) Semi-empirical procedures for evaluating liquefaction potential during earthquakes. In: 11th International Conference on Soil Dynamics and Earthquake Engineering, and 3rd International Conf. on Earthquake Geotechnical Engineering. Berkeley, pp 32–56

Idriss IM, Boulanger RW (2010) SPT-based liquefaction triggering procedure. Center for Geotechnical Modeling, Department of Civil and Environmental Engineering, University of California, Davis, California

Iwasaki T, Tatsuoka F, Tokida K -i., Yasuda S (1978) A practical method for assessing soil liquefaction potential based on case studies at various sites in Japan. In: Proc. of 2nd International Conference on Microzonation. San Francisco, pp 885–896

522 Iwasaki T, Tokida K, Tatsuoka F, et al (1982) Microzonation for soil liquefaction potential using simplified
523 methods. In: Proceedings of 3rd International Earthquake Microzonation Conference. pp 1319–1330

524 Juang CH, Chen CJ, Jiang T, Andrus RD (2000) Risk-based liquefaction potential evaluation using standard
525 penetration tests. Canadian Geotechnical Journal 37:1195–1208. doi: 10.1139/t00-064

526 Juang CH, Jiang T, Andrus RD (2002) Assessing Probability-based Methods for Liquefaction Potential Evaluation.
527 Journal of Geotechnical and Geoenvironmental Engineering 128:580–589

528 Juang CH, Yuan H, Lee D-H, Lin P-S (2003) Simplified cone penetration test-based method for evaluating
529 liquefaction resistance of soils. Journal of Geotechnical and Geoenvironmental Engineering 129:66–80. doi:
530 10.1061/(ASCE)1090-0241(2003)129:1(66)

531 Kayen RE, Mitchell JK, Seed RB, et al (1992) Evaluation of SPT-, CPT-, and shear wave-based methods for
532 liquefaction potential assessment using Loma Prieta data. In: Proceedings of 4th Japan-U.S. Workshop on
533 Earthquake-Resistant Des. of Lifeline Fac. and Countermeasures for Soil Liquefaction. pp 177–204

534 Ku CS, Lee DH, Wu JH (2004) Evaluation of soil liquefaction in the Chi-Chi, Taiwan earthquake using CPT. Soil
535 Dynamics and Earthquake Engineering 24:659–673. doi: 10.1016/j.soildyn.2004.06.009

536 Lee YF, Chi YY, Lee DH, et al (2007) Simplified models for assessing annual liquefaction probability - A case
537 study of the Yuanlin area, Taiwan. Engineering Geology 90:71–88. doi: 10.1016/j.enggeo.2006.12.003

538 Marcuson WF (1978) Definition of terms related to liquefaction. Journal of the Geotechnical Engineering Division
539 104:1197–1200

540 Middlemiss CS (1885) Report on the Bengal earthquake of July 14, 1885. Records of Geological Survey of India 8
541 (4):200–221

542 Morgan JP, McIntire WG (1959) Quaternary geology of the Bengal Basin, East Pakistan and India. Bulletin of the
543 Geological Society of America 70:319–342

544 Morino M, Kamal ASMM, Akhter SH, et al (2014a) A paleo-seismological study of the Dauki fault at Jaflong,
545 Sylhet, Bangladesh: Historical seismic events and an attempted rupture segmentation model. Journal of Asian
546 Earth Sciences 91:218–226. doi: 10.1016/j.jseaes.2014.06.002

Morino M, Kamal ASMM, Muslim D, et al (2011) Seismic event of the Dauki Fault in 16th century confirmed by trench investigation at Gabrakhari Village, Haluaghat, Mymensingh, Bangladesh. Journal of Asian Earth Sciences 42:492–498. doi: 10.1016/j.jseaes.2011.05.002

Morino M, Monsur MH, Kamal ASMM, et al (2014b) Examples of paleo-liquefaction in Bangladesh. The Journal of the Geological Society of Japan 120:VII–VIII. doi: 10.5575/geosoc.2014.0032

Oldham RD (1899) Report on the great earthquake of 12th June 1897. Memoirs of the Geological Survey of India 29:1–379

Olsen RS (1997) Cyclic liquefaction based on the cone penetration test. In: Proceeding of NCEER workshop on evaluation of liquefaction resistance of soils. National Center for Earthquake Engineering Research, State University of New York, Buffalo, pp 225–276

Olsen RS (1988) Using the CPT for dynamic response characterization. In: Proceedings of the Earthquake Engineering and Soil Dynamics II Conference. American Society of Civil Engineers, New York, pp 111–117

Olsen RS, Koester JP (1995) Prediction of liquefaction resistance using the CPT. In: Proceedings of the International Symposium on Cone Penetration Testing, CPT'95, Linkoping, Sweden, Vol. 2. SGS. pp 251–256

Rahman M, Siddiqua S, Kamal A (2015) Liquefaction hazard mapping by liquefaction potential index for Dhaka City, Bangladesh. Engineering Geology 188:137–147. doi: 10.1016/j.enggeo.2015.01.012

Rahman MZ, Siddiqua S (2017) Evaluation of liquefaction-resistance of soils using standard penetration test, cone penetration test, and shear-wave velocity data for Dhaka, Chittagong, and Sylhet cities in Bangladesh. Environmental Earth Sciences 76:207. doi: 10.1007/s12665-017-6533-9

Rahman MZ, Siddiqua S, Kamal ASMM (2021) Site response analysis for deep and soft sedimentary deposits of Dhaka City, Bangladesh. Natural Hazards. doi: 10.1007/s11069-021-04543-w

Rahman MZ, Siddiqua S, Kamal ASMM (2020) Seismic source modeling and probabilistic seismic hazard analysis for Bangladesh. Springer Netherlands

Reimann K-U (1993) Geology of Bangladesh. Gebruder Borntraeger Verlagsbuchhandlung, Science Publishers, Berlin

572 Robertson PK, Campanella RG (1985) Liquefaction potential of sands using the CPT. Journal of Geotechnical
573 Engineering 111:384–403

574 Robertson PK, Wride CE (1998) Evaluating cyclic liquefaction potential using the cone penetration test. Canadian
575 Geotechnical Journal 35:442–459. doi: 10.1139/t98-017

576 Sassa S, Takagawa T (2019) Liquefied gravity flow-induced tsunami: first evidence and comparison from the 2018
577 Indonesia Sulawesi earthquake and tsunami disasters. Landslides 16:195–200. doi: 10.1007/s10346-018-1114-
578 x

579 Seed HB, de Alba P (1986) Use of SPT and CPT tests for evaluating the liquefaction resistance of sands. In:
580 Clemence SP (ed) Use of in situ tests in geotechnical engineering. American Society of Civil Engineers,
581 Geotechnical Special Publication 6, pp 281–302

582 Seed HB, Idriss IM (1967) Analysis of Soil Liquefaction: Niigata Earthquake. Journal of the Soil Mechanics and
583 Foundations Division 93:83–108

584 Seed HB, Idriss IM (1971) Simplified procedure for evaluating soil liquefaction potential. Journal of Soil Mechanics
585 and Foundations Division 97:1249–1273

586 Seed HB, Idriss IM (1982) Ground motions and soil liquefaction during earthquakes. Earthquake Engineering
587 Research Institute Monograph, Oakland

588 Seed HB, Idriss IM, Arango I (1983) Evaluation of liquefaction potential using field performance data. Journal of
589 Geotechnical Engineering 109:458–482

590 Seed HB, Tokimatsu K, Harder Jr. LF, Chung R (1984) The Influence of SPT procedures on soil liquefaction
591 resistance evaluations. Report No. UCB/EERC-84/15, Earthquake Engineering Research Center, University of
592 California, Berkeley

593 Seed HB, Tokimatsu K, Harder LF, Chung RM (1985) Influence of SPT procedures in soil liquefaction resistance
594 evaluations. Journal of Geotechnical Engineering 111:1425–1445. doi: 10.1061/(ASCE)0733-
595 9410(1985)111:12(1425)

596 Sonmez H, Gokceoglu C (2005) A liquefaction severity index suggested for engineering practice. Environmetal

597 Geology 48:81–91. doi: 10.1007/s00254-005-1263-9

598 Stark TD, Olson SM (1995) Liquefaction resistance using CPT and field case histories. Journal of Geotechnical
599 Engineering ASCE, 121:856–869

600 Steckler MS, Akhter SH, Seeber L (2008) Collision of the Ganges-Brahmaputra Delta with the Burma Arc:
601 Implications for earthquake hazard. Earth and Planetary Science Letters 273:367–378. doi:
602 10.1016/j.epsl.2008.07.009

603 Steckler MS, Mondal DR, Akhter SH, et al (2016) Locked and loading megathrust linked to active subduction
604 beneath the Indo-Burman Ranges. Nature Geoscience 9:615–618. doi: 10.1038/ngeo2760

605 Stuart M (1920) The Srimangal earthquake of 8th July 1918. Memoirs of the Geological Survey of India 46 (1):1–70

606 Wang Y, Sieh K, Tun ST, et al (2014) Active tectonic and earthquake Myanmar region. Journal of Geophysical
607 Research: Solid Earth 119:3767–3822. doi: 10.1002/2013JB010762.Received

608 Yeats RS, Sieh K, Allen CR (1997) The Geology of Earthquakes. Oxford University Press

609 Youd BTL, Idriss IM, Andrus RD, et al (2001) Liquefaction resistance of soils: summary report from the 1996
610 NCEER and 1998 NCEER/NSF workshops on evaluation of liquefaction resistance of soils. Jounral of
611 Geotechnical and Geoenvironmental Engineering 127:817–833

612

Figures

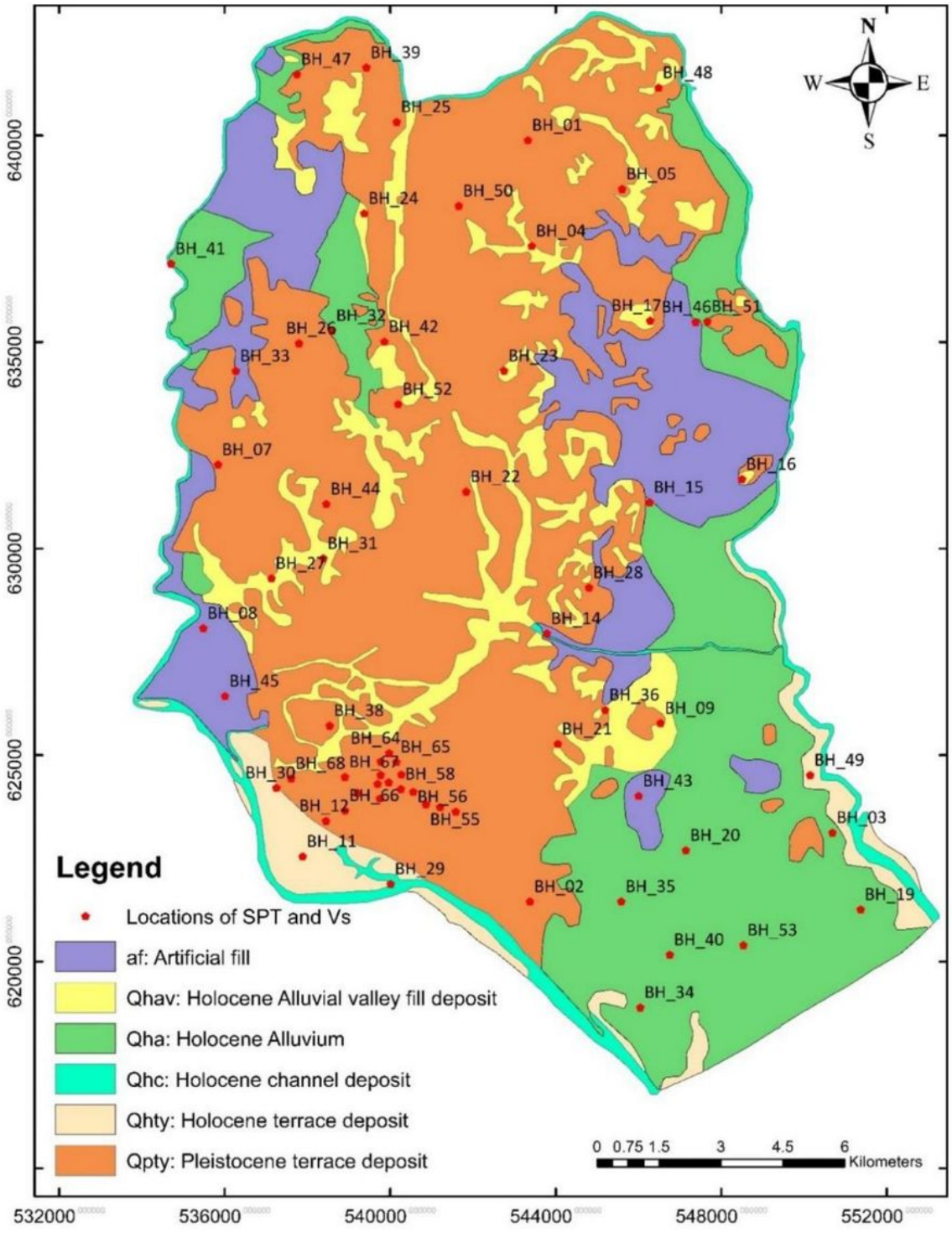

Figure 1

Surface geological map of Dhaka City with locations of the boreholes (modified from Rahman et al. (2015)) Note: The designations employed and the presentation of the material on this map do not imply the expression of any opinion whatsoever on the part of Research Square concerning the legal status of

any country, territory, city or area or of its authorities, or concerning the delimitation of its frontiers or boundaries. This map has been provided by the authors.

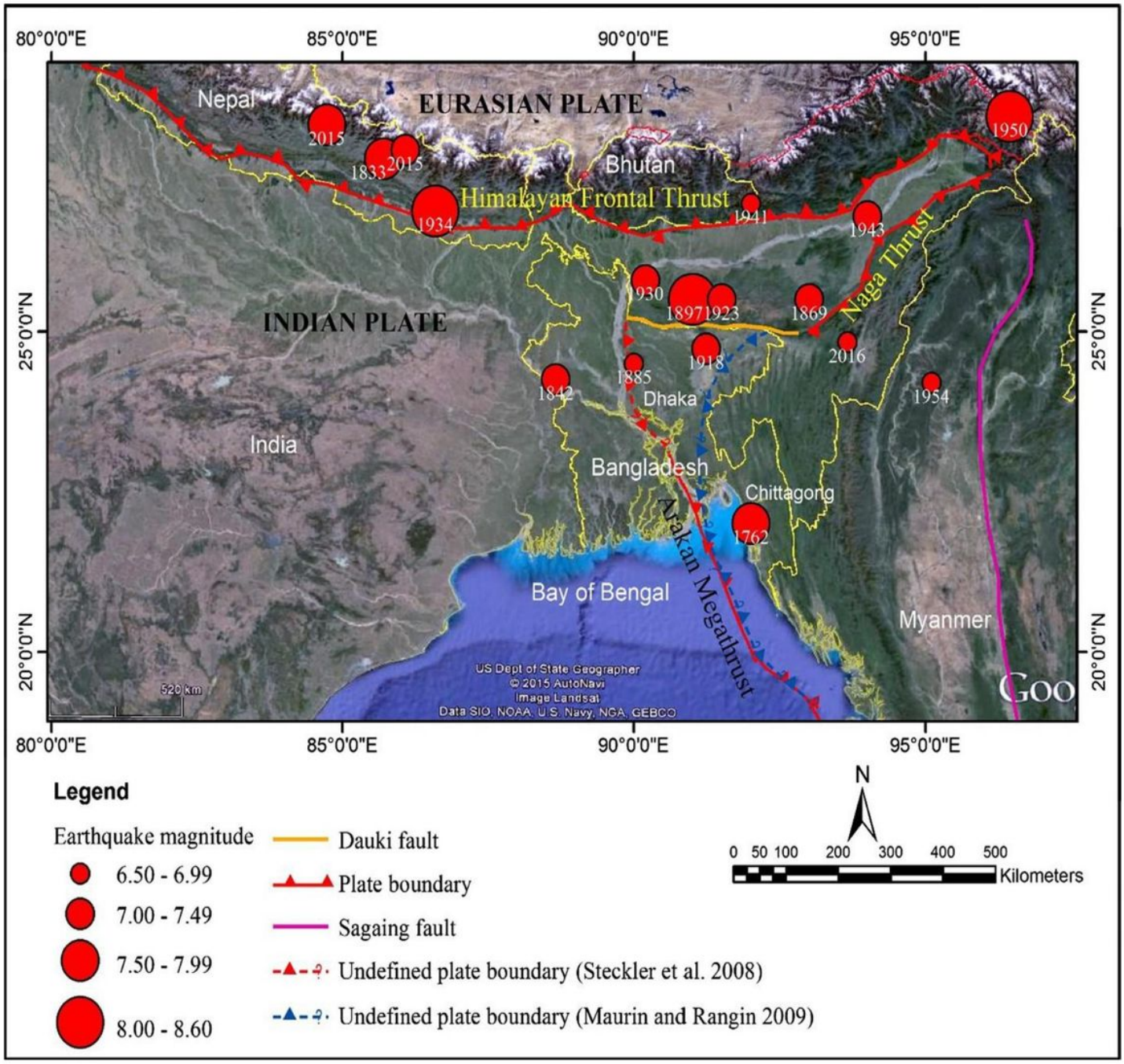

Figure 2

Recent and historical earthquakes of magnitude greater than Mw 6.5 from 1762 and 2016 (retrieved from Rahman and Siddiqua (2017)) Note: The designations employed and the presentation of the material on this map do not imply the expression of any opinion whatsoever on the part of Research Square concerning the legal status of any country, territory, city or area or of its authorities, or concerning the delimitation of its frontiers or boundaries. This map has been provided by the authors.

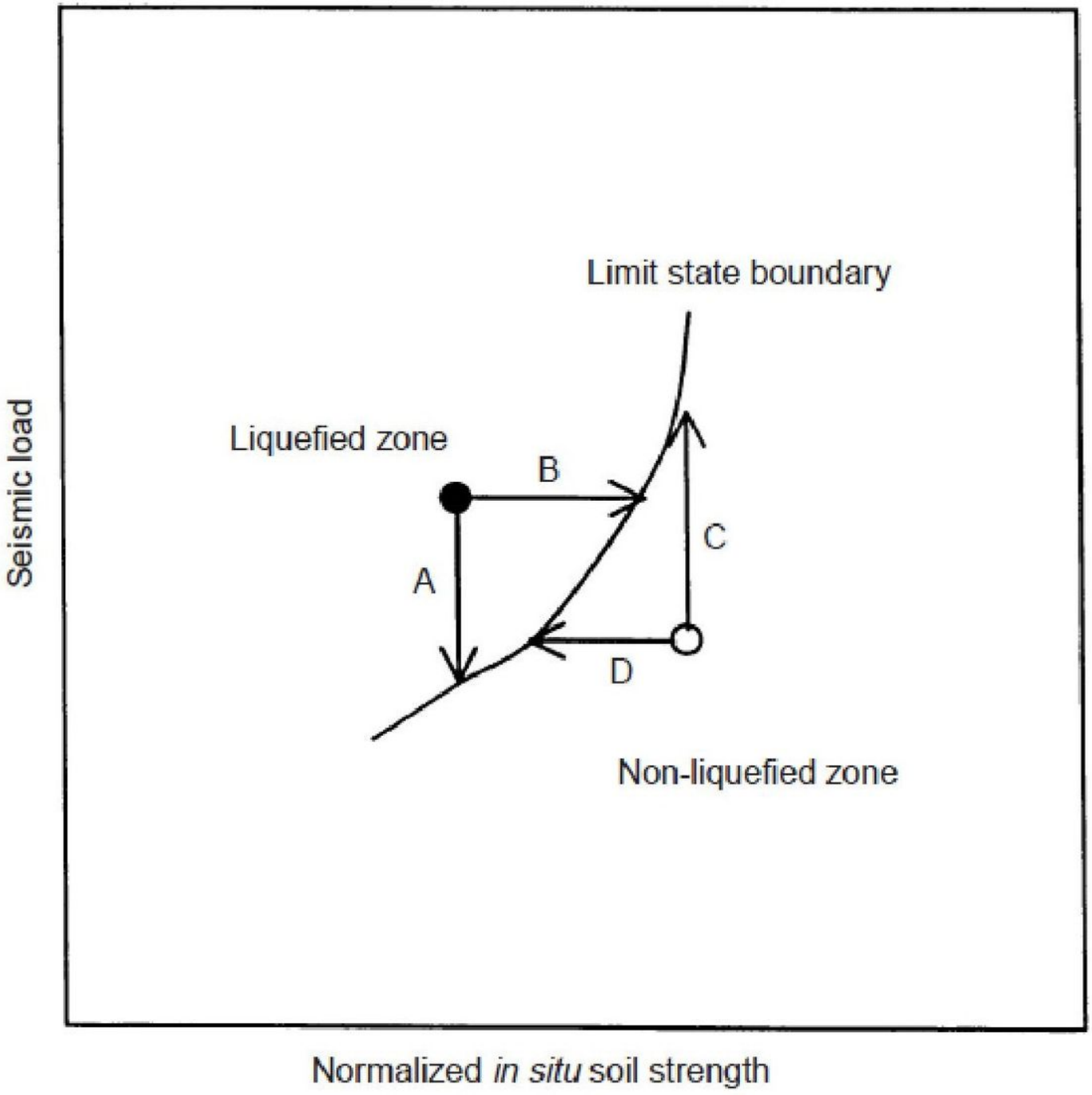

Figure 3

Conceptual model of the mechanism to search limit state boundary (after Chen and Juang, (2000))

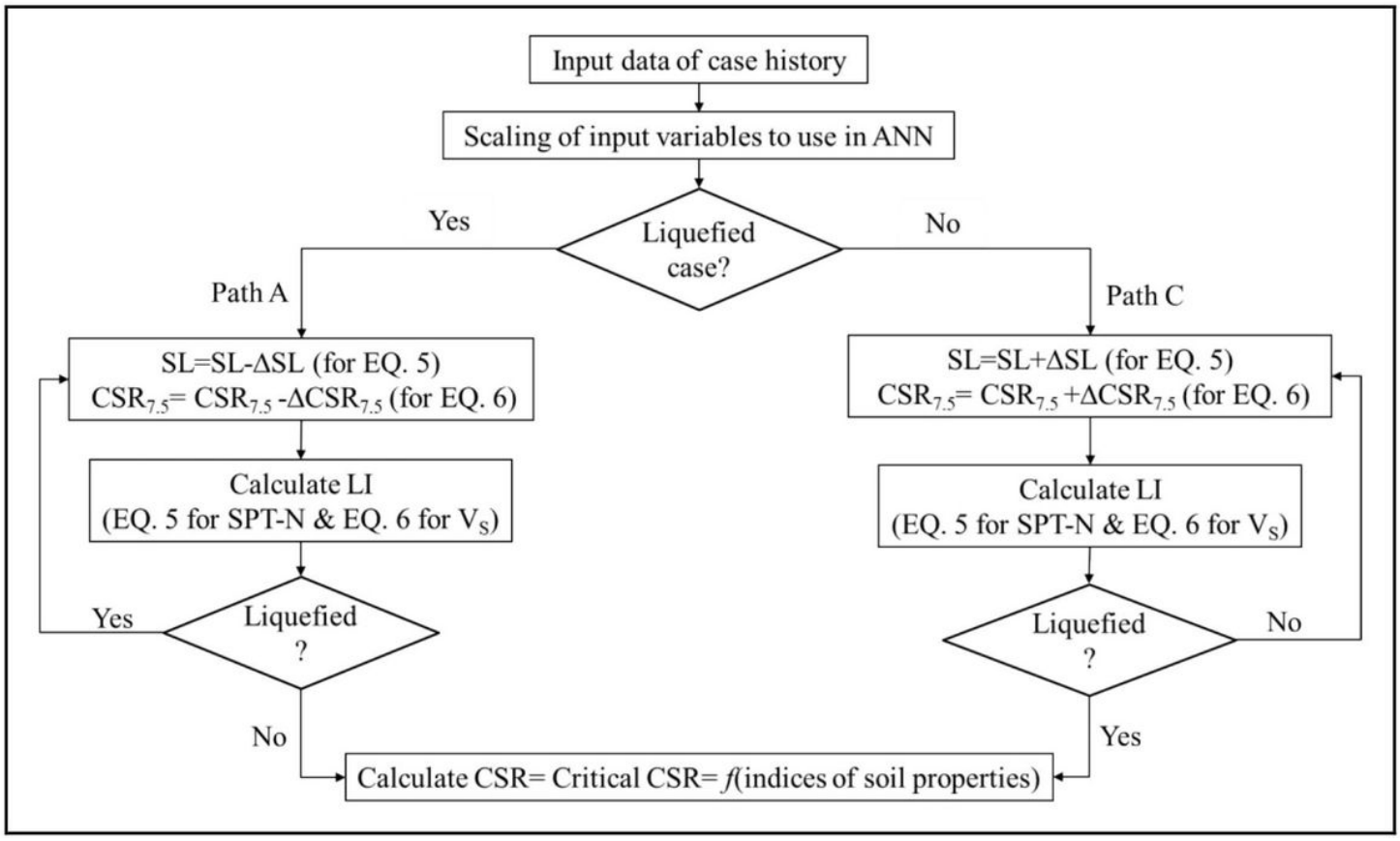

Figure 4

Searching mechanism of critical cyclic stress ratio (CSR) (after Juang et al. (2000))

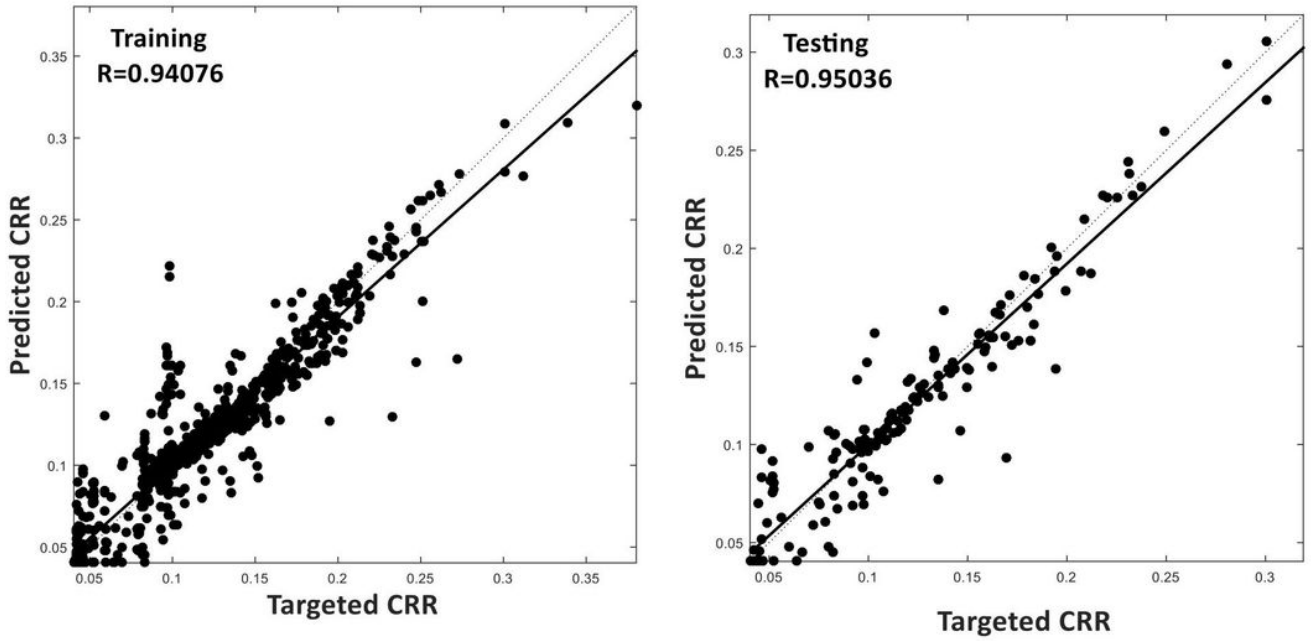

Figure 5

Performance of CRRSPT model

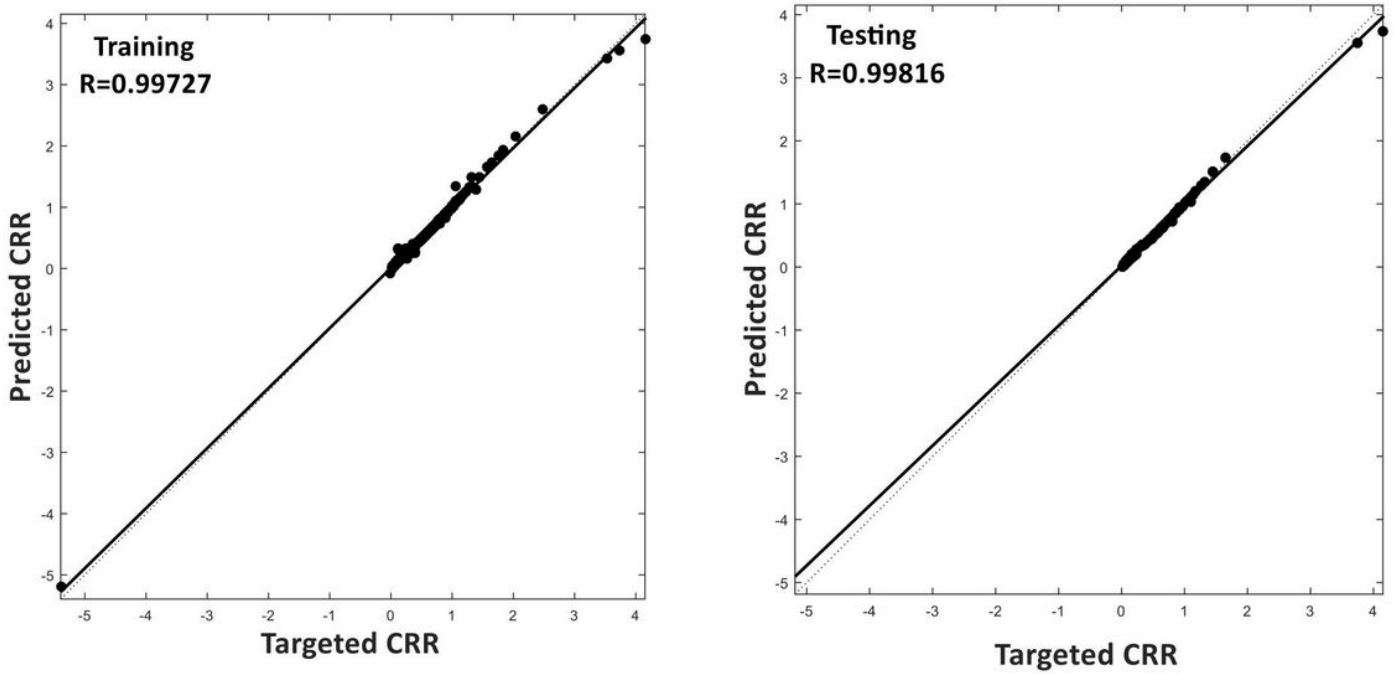

Figure 6

Performance of CRRVs model

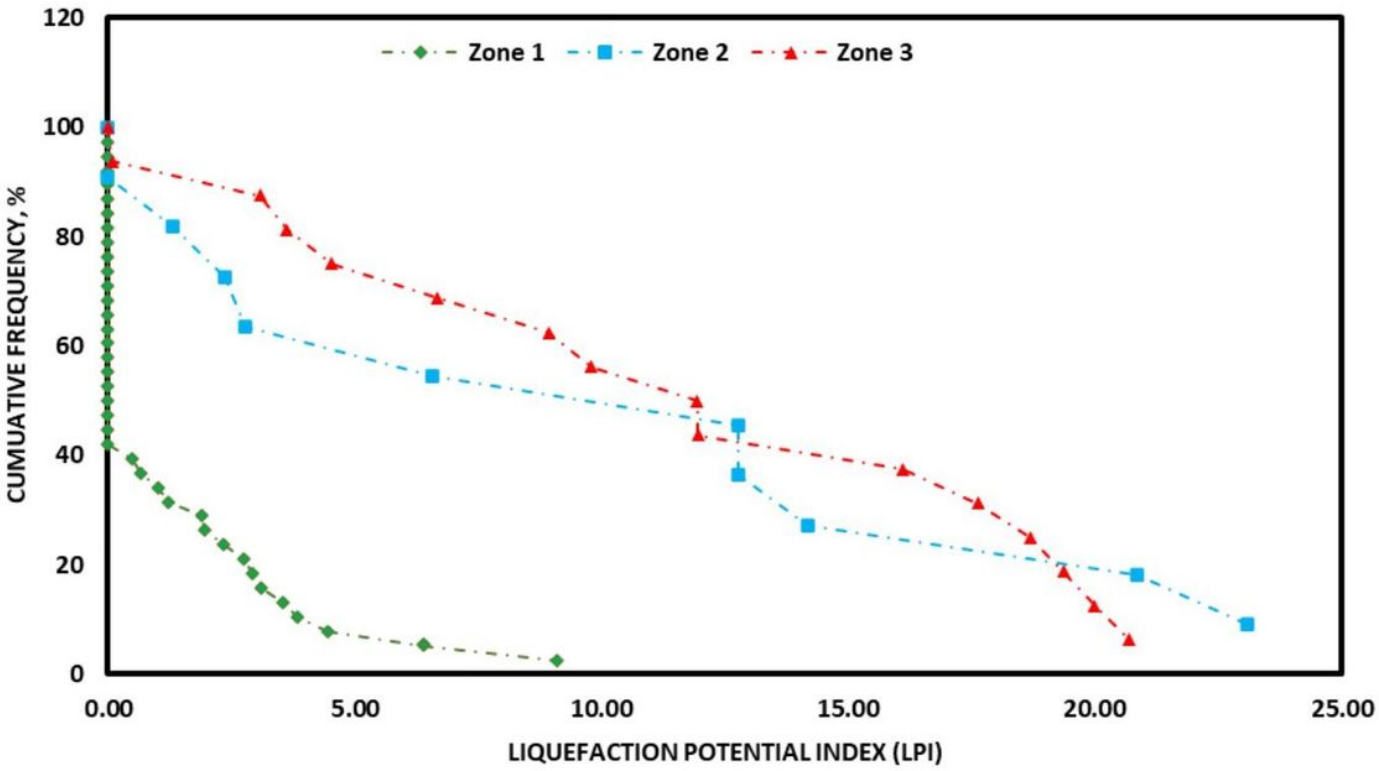

Figure 7

Cumulative frequency (CF) distribution of LPI values of SPT-N data for each liquefaction hazard zone of Dhaka City

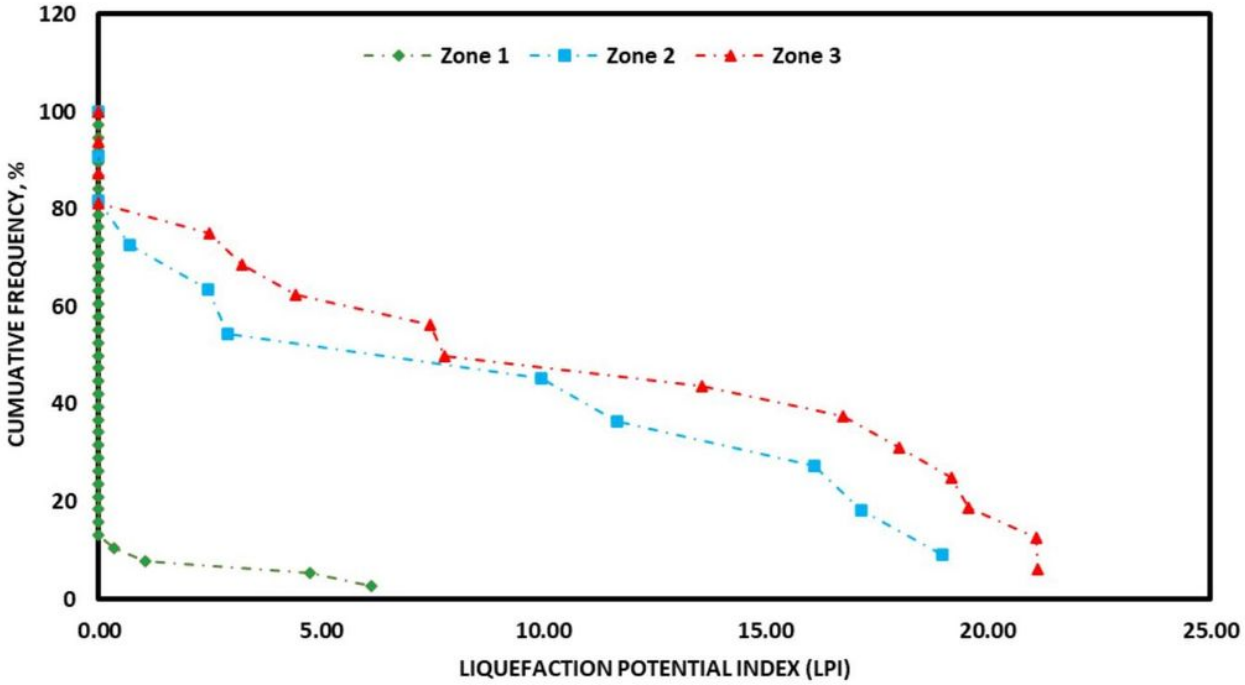

Figure 8

Cumulative frequency (CF) distribution of LPI values of Vs data for each liquefaction hazard zone of Dhaka City

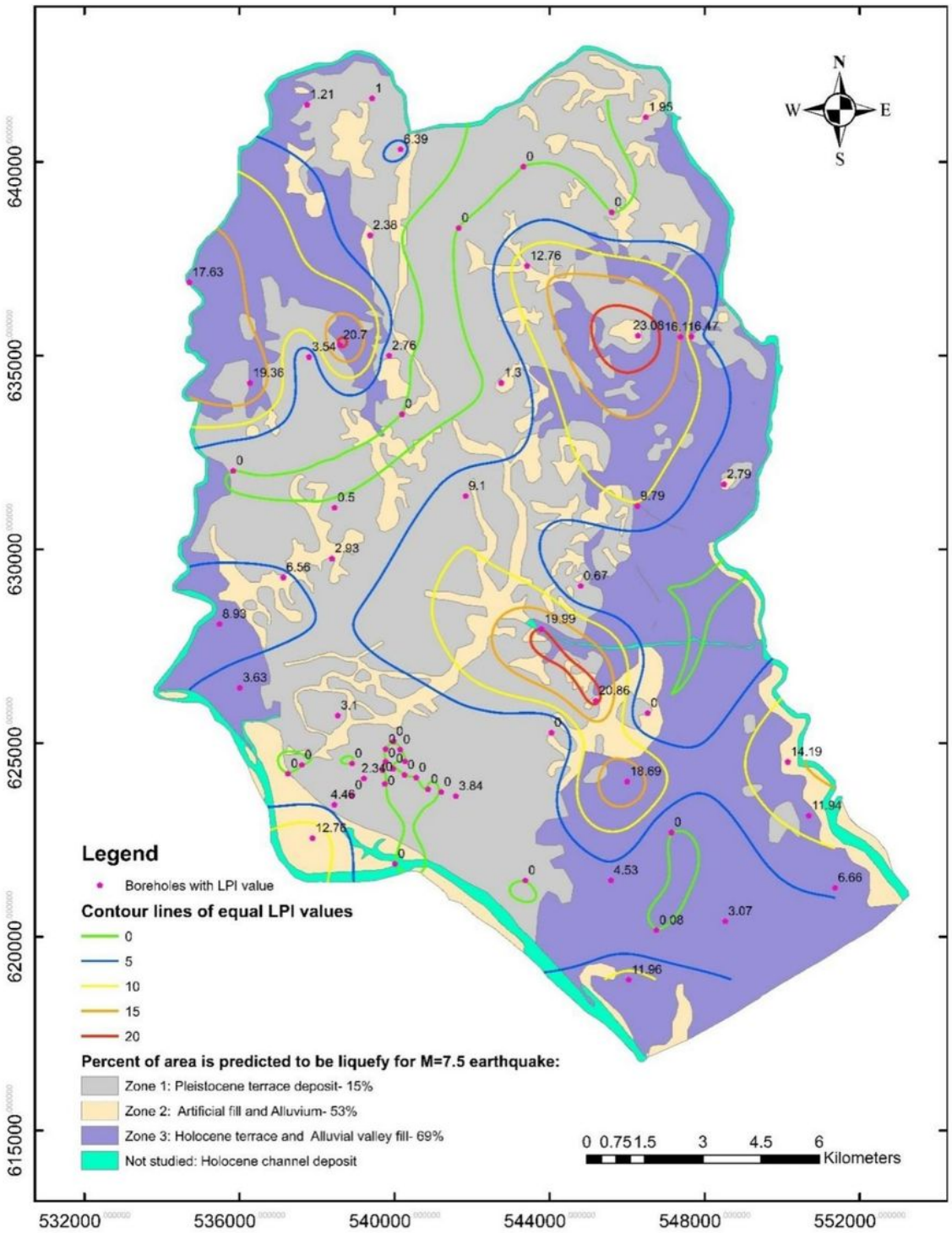

Figure 9

Liquefaction hazard map for Dhaka City using the LPI values of the SPT-N data for a scenario earthquake of Mw 7.5 with a peak horizontal ground acceleration (PGA) of 0.15 g. According to Iwasaki et al. (1982), liquefaction hazard for LPI > 15 is very high, for 5 < LPI≤ 15 is high, for 0 <LPI ≤ 5 is low; and for LPI = 0 is very low. According to Holzer et al. (2006), the cumulative frequency (CF) distributions of the LPI of three zones indicate that 15%, 53%, and 69% of areas of Zone 1, 2, and 3, respectively, exhibit surface

manifestation of liquefaction Note: The designations employed and the presentation of the material on this map do not imply the expression of any opinion whatsoever on the part of Research Square concerning the legal status of any country, territory, city or area or of its authorities, or concerning the delimitation of its frontiers or boundaries. This map has been provided by the authors.

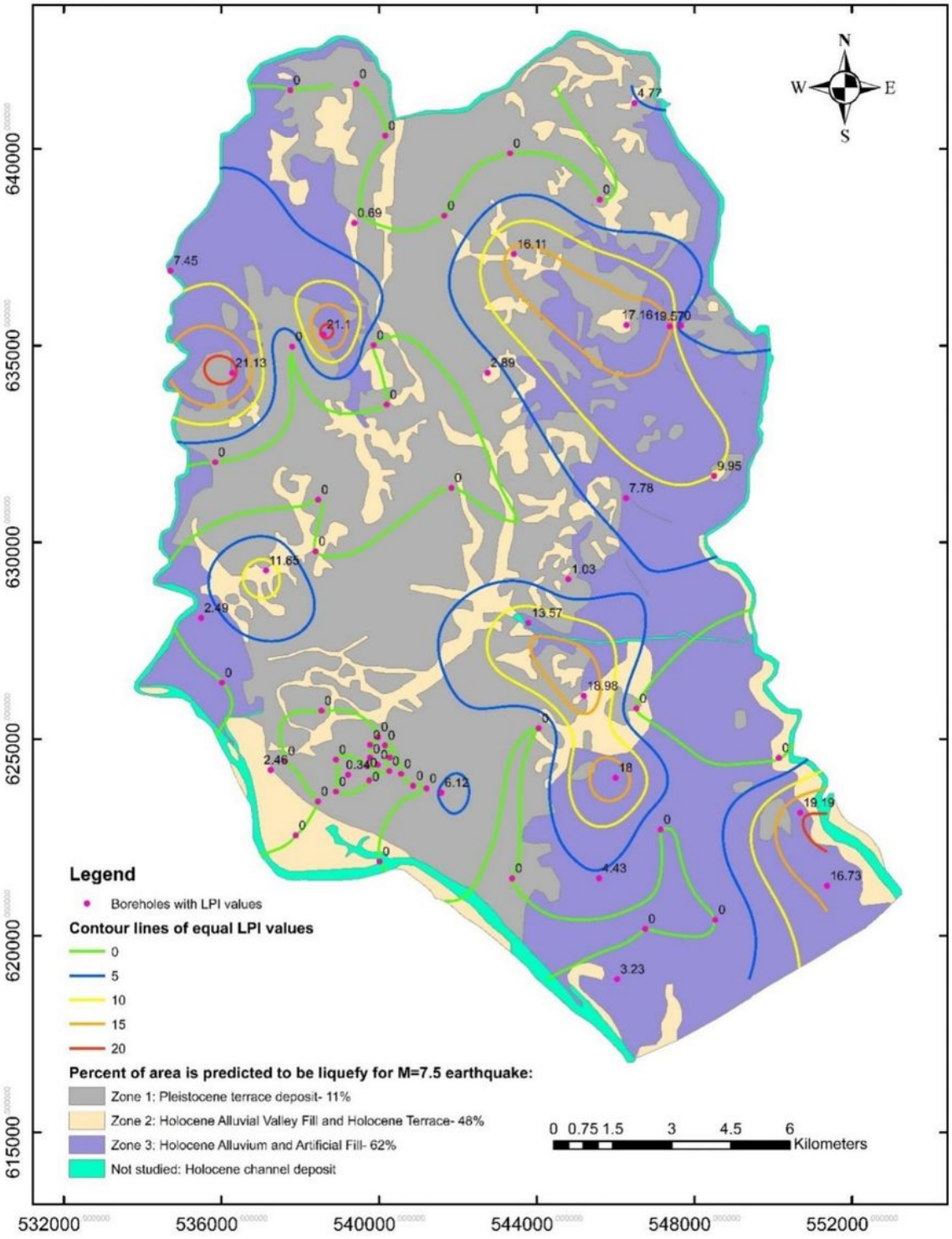

Figure 10

Liquefaction hazard map for Dhaka City using the LPI values of the Vs data for a scenario earthquake of Mw 7.5 with a peak horizontal ground acceleration (PGA) of 0.15 g. According to Iwasaki et al. (1982), liquefaction hazard for LPI > 15 is very high, for 5 < LPI≤ 15 is high, for 0 <LPI ≤ 5 is low; and for LPI = 0 is very low. According to Holzer et al. (2006), the cumulative frequency (CF) distributions of the LPI of three zones indicate that 15%, 53%, and 69% of areas of Zone 1, 2, and 3, respectively, exhibit surface manifestation of liquefaction Note: The designations employed and the presentation of the material on this map do not imply the expression of any opinion whatsoever on the part of Research Square concerning the legal status of any country, territory, city or area or of its authorities, or concerning the delimitation of its frontiers or boundaries. This map has been provided by the authors.

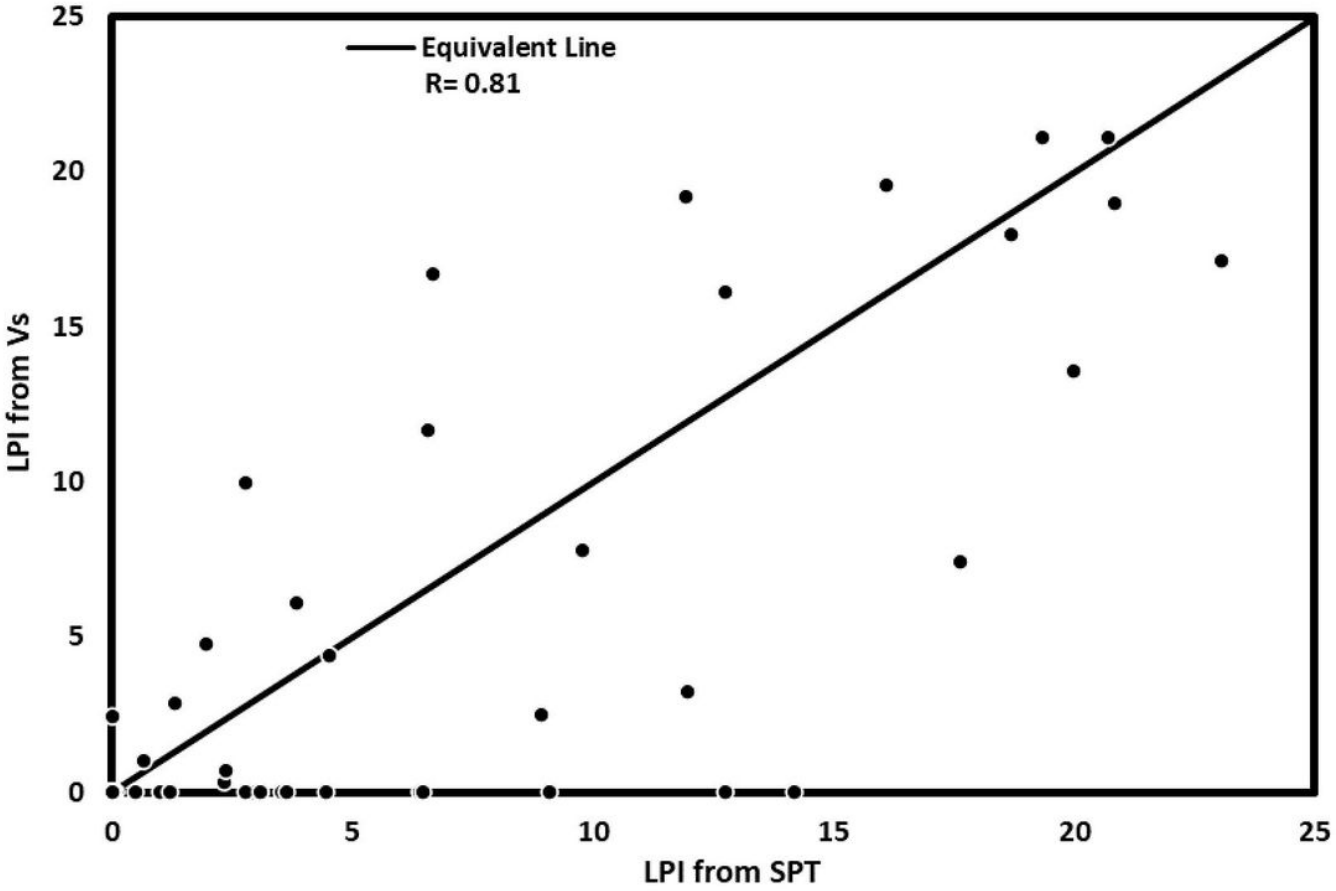

Figure 11

Comparison between LPI values of SPT-N and Vs datasets